# Reconstruction of the mouse extrahepatic biliary tree using primary human extrahepatic cholangiocyte organoids

**Extrahepatic cholangiocyte organoids for cell-based therapy applications**

Fotios Sampaziotis[1,2,3], Alexander W Justin[4], Olivia C. Tysoe[1,2], Steve Sawiak[5†], Edmund M Godfrey[6†], Sara S Upponi[6†], Richard L. Gieseck III[7], Miguel Cardoso de Brito[1], Natalie Lie Berntsen[8], María J Gómez-Vázquez[9], Daniel Ortmann[1], Loukia Yiangou[1], Alexander Ross[1,10,11], Johannes Bargehr[1,12], Alessandro Bertero[1], Mariëlle CF Zonneveld[1], Marianne T Pedersen[13], Matthias Pawlowski[1], Laura Valestrand[7,14,15], Pedro Madrigal[1], Nikitas Georgakopoulos[2], Negar Pirmadjid[2], Gregor M Skeldon[16,17], John Casey[18], Wenmiao Shu[16,17], Paulina M Materek[1], Kirsten E Snijders[1], Stephanie E Brown[1], Casey A Rimland[1,2,7,19], Ingrid Simonic[20], Susan E Davies[21], Kim B Jensen[13], Matthias Zilbauer[10,11,22], William TH Gelson[3], Graeme Alexander[23], Sanjay Sinha[1,12], Nicholas RF Hannan[24], Thomas Wynn[7], Tom H Karlsen[8], Espen Melum[8], Athina E. Markaki[4], Kourosh Saeb-Parsy[2*], Ludovic Vallier[1,2,25*]

[1]Wellcome Trust-Medical Research Council Stem Cell Institute, Cambridge Stem Cell Institute, Anne McLaren Laboratory, Department of Surgery, University of Cambridge, Cambridge, UK

[2]Department of Surgery, University of Cambridge and NIHR Cambridge Biomedical Research Centre, Cambridge, UK

[3]Department of Hepatology, Cambridge University Hospitals NHS Foundation Trust, Cambridge, UK

[4]Department of Engineering, University of Cambridge, Cambridge, UK

[5]Department of Clinical Neurosciences, University of Cambridge, Cambridge, UK

[6]Department of Radiology, Cambridge University Hospitals NHS Foundation Trust, Cambridge, UK

[7]Immunopathogenesis Section, Laboratory of Parasitic Diseases, National Institute of Allergy and Infectious Diseases, National Institutes of Health, Bethesda, Maryland, USA

[8]Norwegian PSC Research Center, Division of Surgery, Inflammatory Medicine and Transplantation, Oslo University Hospital, Rikshospitalet, Oslo.

[9]Cambridge Genomic Services, Department of Pathology, University of Cambridge, Cambridge, UK

[10]University Department of Paediatrics, University of Cambridge, Cambridge, UK

[11]Department of Paediatric Gastroenterology, Hepatology and Nutrition, Cambridge University Hospitals NHS Foundation Trust, Cambridge, UK

[12]Division of Cardiovascular Medicine, University of Cambridge, Cambridge, UK

[13]Biotech Research and Innovation Centre (BRIC), University of Copenhagen, Copenhagen, Denmark

[14]Research Institute of Internal Medicine, Division of Surgery, Inflammatory Medicine and Transplantation, Oslo University Hospital, Rikshospitalet, Oslo,

[15]Institute of Clinical Medicine, University of Oslo, Oslo.

[16]School of Engineering and Physical Sciences, Heriot-Watt University, United Kingdom

[17]Department of Biomedical Engineering, University of Strathclyde, United Kingdom

[18]Department of Surgery, University of Edinburgh, Edinburgh Royal Infirmary, Edinburgh, EH16 4SU, United Kingdom

[19]University of North Carolina, Chapel Hill School of Medicine, Chapel Hill, North Carolina, USA

[20]Medical Genetics Laboratories, Cambridge University Hospitals NHS Trust, Cambridge, UK

[21]Department of Histopathology, Cambridge University Hospitals NHS Foundation Trust, Cambridge, UK

[22]Wellcome Trust-Medical Research Council Stem Cell Institute, Cambridge Stem Cell Institute, University of Cambridge, Cambridge, UK

[23]Department of Medicine, School of Clinical Medicine, University of Cambridge, Cambridge, UK

[24]Center for Biomolecular Sciences, University of Nottingham, UK

[25]Wellcome Trust Sanger Institute, Hinxton, UK

**Authorship note:** * Kourosh Saeb-Parsy and * Ludovic Vallier contributed equally to this work.

[†]Stephen Sawiak, [†]Edmund Godfrey and [†]Sara Upponi contributed equally to this work.

**Correspondence:** Ludovic Vallier, Laboratory for Regenerative Medicine, West Forvie Building, Robinson Way, University of Cambridge. Cambridge CB2 0SZ, United Kingdom. Telephone: 44.1223.747489; Fax: 44.1223.763.350; E-mail: lv225@cam.ac.uk.

Disorders of the extrahepatic bile ducts carry significant morbidity and mortality. Indeed, 70% of pediatric liver transplantations are performed to treat biliary atresia (1), Primary Sclerosing Cholangitis (PSC) alone accounts for 5% of US liver transplantations (2) and biliary complications are the leading cause of graft failure following deceased liver transplantation (3,4). Treatment options remain limited (5,6) due to the lack of healthy tissue that can be used to reconstruct and replace diseased bile ducts. In vitro expansion of native cholangiocytes could address this challenge and provide cells suitable for tissue engineering applications such as biliary reconstruction. However, the culture of primary biliary epithelium remains problematic (7). Here we report a novel method for the isolation and propagation of primary human cholangiocytes from the extrahepatic biliary tree, compatible with regenerative medicine applications. The resulting Extrahepatic Cholangiocyte Organoids (ECOs) express key biliary markers such as CK7, CK19, GGT, CFTR and maintain their functional properties in vitro including ALP, GGT activity and responses to secretin and somatostatin. The potential of ECOs for tissue engineering and clinical applications is further illustrated by their capacity to populate biodegradable scaffolds, organize into a functional biliary epithelium and rescue a murine model of extrahepatic biliary injury (EHBI).

To establish this system, we first focused on identifying optimal conditions to isolate primary cholangiocytes from the biliary epithelium which forms a monolayer covering the luminal surface of the biliary tree (8). We tested several approaches for recovering these cells and mechanical dissociation by brushing or scraping the bile duct lumen was associated with improved survival compared to enzymatic digestion (Figure 1a, Supplementary Fig. 1a).

Furthermore, the majority of the resulting cells co-expressed the biliary markers Cytokeratin 7 (CK7) and Cytokeratin 19 (CK19) (94.6 ± 2.4% (SD; n=3); while no contamination from mesenchymal cell types was detected. (Supplementary Fig 2). Consequently, mechanical dissociation constitutes the optimal method for harvesting extrahepatic cholangiocytes.

To discern appropriate conditions for the maintenance and propagation of these cells, we optimized our recently established system for 3D culture of human induced pluripotent stem cell-derived intrahepatic cholangiocytes (9). Screening of multiple growth factors known to support expansion of cholangiocytes and epithelial organoids (10,11) (Supplementary Fig 1b-1c) identified that the combination of Epidermal Growth Factor (EGF), R-Spondin and Dickkopf-related protein 1 (DKK-1) promoted the growth of primary cholangiocytes into organoids (Figure 1b, 1c). Due to the paradoxical requirement for both a Wnt potentiator (R-spondin) and an inhibitor (DKK-1), we characterized the canonical and non-canonical/PCP Wnt pathway activity in ECOs. Our results demonstrate increased levels of β-catenin phosphorylation (Supplementary Fig. 1d-1e), signifying reduced WNT canonical pathway activity in ECOs, as well as increased Rho Kinase activity (Supplementary Fig. 1f), which could be consistent with enhanced non-canonical/PCP signaling in ECOs. Thus, it is possible that non-canonical Wnt signaling controls ECO expansion marking a significant difference with previous organoid culture conditions (11).

Under these conditions, we derived 8 different ECO lines (Supplementary Table 1) from a variety of deceased donors aged from 33 to 77 years. Importantly, we obtained similar results by using cholangiocytes isolated from

the gallbladder or by harvesting common bile duct cholangiocytes using an Endoscopic Retrograde Cholangio-Pancreatography (ERCP) brush instead of scrapping the lumen (Supplementary Fig 3). Consequently, ECOs can be derived from different areas of the extra-hepatic biliary tree and harvested using peri-operative (dissection and scrapping) or minimally invasive (ERCP brushings) approaches.

The resulting cells were expanded in vitro for prolonged periods of time (Supplementary Fig 4a) while maintaining their genetic stability (Supplementary Fig 4b-4c). Electron microscopy revealed the presence of characteristic ultrastructural features including cilia, microvilli and tight junctions (12) (Figure 1d, Supplementary Fig 5), while QPCR and immunofluorescence (IF) analyses established the expression of key biliary markers such as CK7, CK19, Hepatocyte Nuclear Factor-1-beta (HNF1B), Gamma Glutamyl-Transferase (*GGT*), Secretin Receptor (SCR), sodium-dependent bile acid transporter (ASBT/SLC10A2), Cystic fibrosis transmembrane conductance regulator (CFTR) and Sox9 (9) (Figure 1e-1f, Supplementary Fig 3c-3d, 6a-6b). Importantly, stem cell markers (POU5F1, NANOG, PROM1, LGR-4/5/6), markers of non-biliary lineages (albumin, α1-antitrypsin, CK18, PDX1, insulin and glucagon) and EMT markers (vimentin, SNA1L and S100A4) were not detected (Supplementary Fig 7a-7c). On the other hand, 98.1% ± 0.9% (SD; n=3) of the cells co-expressed CK7 and CK19 following 20 passages (Supplementary Fig 2) thereby confirming the presence of a near homogeneous population of cholangiocytes.

Transcriptomic analyses (Figure 1g, Supplementary Fig. 8, Supplementary Table 2) revealed that ECOs maintain a stable gene expression profile over

multiple passages (Pearson correlation coefficient for Passage 1 (P1) vs. Passage 20 (P20) r=0.99, Supplementary Fig 8a-b), express key biliary markers and cluster closely to freshly isolated cholangiocytes (Pearson correlation coefficient for Primary Cholangiocytes (PCs) vs. Passage 20 (P20) r=0.92; Figure 1g, Supplementary Fig 8b-8d). Gene ontology analyses confirmed enrichment of pathways characteristic for the biliary epithelium (Supplementary Fig 8e). Considered collectively, these results demonstrate that primary cholangiocytes derived from the extrahepatic biliary tree can be expanded in vitro without losing their original characteristics.

We then decided to further characterize ECOs by focusing on their function following long term culture (20 passages). The biliary epithelium regulates the homeostasis of bile through the transport of ions, water and bile acids (8,13). The secretory capacity of ECOs was interrogated using Rhodamine-123, a fluorescent substrate for the cholangiocyte surface glycoprotein Multidrug Resistance protein-1 (MDR1) (14,15) (Figure 2a-2c). Rhodamine-123 accumulated in the ECO lumen only in the absence of the MDR-1 antagonist verapamil, thereby confirming active secretion through MDR-1 (Figure 2a-2c). Luminal extrusion of bile acids (16) was also demonstrated by showing that the fluorescent bile acid Cholyl-Lysyl-Fluorescein (CLF) was actively exported from ECOs (Figure 2d-2f). Furthermore, ECO ALP and GGT activity was comparable to freshly plated primary cholangiocytes (Figure 2g-2h, Supplementary Fig. 3e-3f). The response of ECOs to secretin and somatostatin was also assessed. Secretin promotes water secretion, distending the bile duct lumen, while somatostatin negates the effects of secretin (17–19). Accordingly, organoids exposed to secretin increased their

diameter compared to untreated controls, while somatostatin inhibited the effect of secretin (Figure 2i-2j). Our data, therefore, demonstrate that ECOs maintain their functional properties after long term culture.

These results prompted us to investigate the interest of ECOs for in vivo use, especially regenerative medicine applications. We first characterized the potential of ECOs for in vivo engraftment and survival by transplanting cells under the kidney capsule of NOD.Cg-Prkdc$^{scid}$ Il2rg$^{tm1Wjl}$ (NSG) mice (Supplementary Fig 9a) for 12 weeks (20). ECOs successfully engrafted forming tubular structures expressing biliary markers such as CK19 (Supplementary Fig 9b-d). Importantly, no tumour formation or markers of differentiation to other lineages were detected (Supplementary Fig 9d). Thus, ECOs appear to maintain their basic characteristics even after prolonged engraftment in vivo under the kidney capsule.

Following these encouraging results, we decided to define the capacity of ECOs to repair the biliary epithelium. For that, we developed a mouse model of extrahepatic biliary injury (EHBI). More specifically, to simulate biliary tree wall defects requiring biliary reconstruction (21), the biliary tree of healthy NSG mice was compromised through a longitudinal incision in the gallbladder wall (Figure 3a). We then generated a bioengineered tissue patch to repair this injury by populating Polyglycolic Acid (PGA) biodegradable scaffolds with either GFP-expressing ECOs (Supplementary Fig 10-12, Supplementary Note) or GFP-expressing fibroblasts (Supplementary Fig 13a-13d). The resulting bioengineered tissue was subsequently transplanted into the injured animals to close the wall defect created by surgery. Animals receiving acellular scaffolds died within 24 hours of the operation (Figure 3b) and post-

mortem examination revealed yellow pigmentation of the peritoneal cavity and seminal vesicles consistent with bile leak (Supplementary Fig 14a); while all animals in fibroblast-scaffold group failed to reconstruct their gallbladder which was replaced by fibrotic tissue incompatible with bile transport or storage (Supplementary Fig 13e-13g). In contrast, animals transplanted with scaffolds containing ECOs survived for up to 104 days without complications and were culled electively (Figure 3b). Importantly, the reconstructed gallbladders in the ECO group were fully remodeled resembling the morphology of their native counterparts (Figure 3c, Supplementary Fig 14b). Histology (Figure 3d), IF and QPCR analyses of the ECO-reconstructed gallbladders (Figure 3e, Supplementary Fig 14c-14d) unveiled integration of GFP-positive ECOs expressing biliary markers, such as CK19, CK7, HNF1B, Sox9, CFTR and a human-specific epitope for Ku80 (Figure 3e, Supplementary Fig 14c). Importantly, these IF analyses also showed the presence of mouse mesenchymal cells expressing vimentin and endothelial cells expressing CD31 in the reconstructed biliary epithelium suggesting that the scaffold is colonized by endogenous cells after transplantation (Supplementary Fig 14c). Interestingly, we also identified a population of GFP+/vimentin+/CK19- cells, suggesting that ECOs may also contribute to the scaffold stroma; possibly through epithelial to mesenchymal transition (EMT; Supplementary Fig 14c, 14e). The integrity of the reconstructed gallbladder lumen and its exposure to bile through continuity with the biliary tree were demonstrated using Magnetic Resonance Cholangio-Pancreatography (MRCP) imaging prior to removal of the organ and was further confirmed with FITC cholangiograms (Figure 3f-3g, Supplementary Fig

14f, Supplementary Video 1). Post mortem surgical examination and full body Magnetic resonance Imaging 104 days post transplantation revealed no evidence of tumor formation (Supplementary Fig 14f, Supplementary Video 2) while IF analyses revealed no GFP+ cells in the adjacent liver tissue (data not shown). On the contrary, gallbladders reconstituted with fibroblasts controls exhibited obliteration of the gallbladder lumen (Supplementary Fig 13h-13i) and replacement of the lumen and biliary epithelium by fibroblasts expressing Fibroblast Specific Antigen S100A4 (Supplementary Fig. 13i-13j). Considered collectively, our findings demonstrate the capacity of ECOs to colonize their physiological niche and regenerate part of the biliary tree without any complications.

Reconstruction of the gallbladder wall provided proof-of-principle for the capacity of ECOs to regenerate the biliary epithelium after injury; however, the majority of extrahepatic bile duct disorders affect the common bile duct (CBD). Therefore we decided to explore the possibility to replace the native CBD of NSG mice with a bioengineered duct consisting of an ECO-populated densified collagen tube. (Supplementary results, Supplementary Fig 15, 16, Fig 4a). A mid-portion of the native CBD was removed and an ECO-populated collagen tube was anastomosed end-to-end to the proximal and distant duct remnants (n=4 animals). Fibroblast populated tubes were used as a negative control (n=4). Biliary reconstruction was achieved in all animals transplanted with ECO-populated tubes (Figure 4b-4c, Supplementary Fig 17a-17d), which were followed up for up to a month post transplantation (Supplementary Fig 17d). Histology and IF analyses revealed a patent lumen, with formation of a biliary epithelium by the transplanted GFP+ cells (Figure 4e-4f,

Supplementary Fig 17a-17b). IF and QPCR analyses confirmed the expression of biliary markers, such as CK19, CK7, HNF1B, CFTR, Sox9 (Figure 4d, 4f, Supplementary Fig 17b) by the engrafted cells but also illustrated the presence of mouse stromal and endothelial cells (Supplementary Fig 17b). Moreover, we observed minimal apoptosis and proliferation in the transplanted tubes 1 month after transplantation, confirming the stability and integrity of the reconstituted biliary epithelium (Supplementary Fig 17b-17c). Lumen patency was further confirmed by FITC-cholangiogram and MRCP (Figure 4g, Supplementary Fig 17f) and all the animals receiving ECO-populated tubes exhibited no increase in serum cholestasis markers (Bilirubin, ALP; Supplementary Fig 17e) accordingly; while the bio-artificial common bile ducts retained their ALP activity in vivo (Figure 4h). On the contrary, all the fibroblast-populated collagen tubes failed due to lumen occlusion (Figure 4b-4c, 4e-4g, Supplementary Fig 17d), resulting in increased biliary pressures and bile leak through the site of anastomosis (Figure 4b). In conclusion, our results demonstrate the capacity of ECO-populated collagen tubes to replace the native CBD in vivo.

In summary, we have demonstrated that epithelial cells from the extrahepatic biliary tree can be expanded and propagated in vitro while maintaining their cholangiocyte transcriptional signature and functional characteristics. In addition, our results show that primary cholangiocytes expanded in vitro as organoids have a unique potential for organ regeneration. Indeed, our system provides the first proof-of-principle for the application of regenerative medicine in the context of common bile duct pathology. The capacity to replace a diseased common bile duct with an in vitro bio-engineered ECO-tube could

have a significant impact for the management of disorders such as biliary atresia, which constitutes the leading cause for pediatric liver transplantation (1); or ischemic strictures which are one of the most common complications following transplantation (3). Consequently ECO-populated scaffolds constitute a novel system with increased clinical relevance in the field of cholangiopathies.

Furthermore, studies of the extrahepatic biliary epithelium have been limited by technical challenges in long-term culture and significant expansion of primary cholangiocytes. These challenges have so far precluded large scale experiments such as transcriptomic and genome-wide analyses which are urgently needed to better understand bile duct diseases, such as PSC and cholangiocarcinoma. The capacity of ECOs for large scale expansion, could address this challenge. Indeed, we demonstrate that starting from $10^5$ extrahepatic cholangiocytes we can generate between $10^{20} - 10^{25}$ cells after 20 passages. Therefore, ECOs not only represent a novel source of cells for cell based therapy but also provide a unique model system for studying the physiology and modeling disorders of the extrahepatic biliary tree in vitro.

Access to human tissue constitutes a significant limitation for systems based on primary cells. However, we show that ECOs can be obtained not only from the common bile duct but also from the gallbladder. Gallbladder tissue is easily accessible and routinely discarded following liver transplantation and cholecystectomy, one of the most common surgical procedures performed. Furthermore, in patients not having surgery the common bile duct can be accessed using minimally invasive procedures, such as Endoscopic Retrograde Cholangio-Pancreatography (ERCP) and we demonstrate that

cholangiocytes can be obtained through brushings, which are routinely performed to acquire histology specimens. Importantly, no morphological or functional differences were observed between organoids obtained with these different methods. Moreover, due to the scalability of our system only a small amount of starting material is required. Finally, recent progress in replacing Matrigel by custom made hydrogels to grow gut organoids (22) suggest that translating our system from Matrigel to Good Manufacturing Practice (GMP) could be feasible. Considered together, these approaches address any issues of tissue availability and open the possibility of autologous as well as allogeneic cell based therapy.

Importantly, the derivation of primary hepatic stem cells using an organoid culture system has been reported previously (11). However, the capacity of the resulting cells to differentiate into functional cholangiocytes and populate the biliary tree in vivo remains to be demonstrated. Furthermore, in vivo applications of such platforms could be restricted by contaminating stem cells with a capacity to proliferate inappropriately after transplantation and /or differentiate into non-biliary cell types. Importantly, despite the association between organoids and adult stem cells (23), we never observed the expression of hepatocyte or pancreatic markers during our experiments either in vitro or after transplantation, suggesting that the differentiation capacity of ECOs is limited to their lineage of origin. Moreover, canonical WNT signaling, which is crucial for the expansion of adult stem cell organoids (24) is blocked in our culture conditions through the use of DKK-1 and further studies may be required to fully elucidate the role of R-spondin in our system. Considered together, these observations suggest that our culture system does not include

1    a stem cell population. However, we cannot completely exclude that these

2    cells could represent a biliary progenitor population based on their ability to

3    self-propagate and generate organoids from single cells (Supplementary

4    Video 3).

5    In conclusion, our results open up novel avenues for the use of extrahepatic

6    primary biliary tissue as a novel platform for in vitro studies, disease modeling

7    and cell based therapy applications.

8

**1**   **Online Methods**

**2**   **Primary biliary tissue**

**3**   Primary biliary tissue (bile duct or gallbladder) was obtained from deceased

**4**   organ donors from whom organs were being retrieved for transplantation. The

**5**   gallbladder or a section of the bile duct was excised during the organ retrieval

**6**   operation after obtaining informed consent from the donor's family (REC

**7**   reference numbers: 09/H0306/73, NRES Committee East of England –

**8**   Norfolk, 12/EE/0253, NRES Committee East of England - Cambridge Central

**9**   and 15/EE/0152 NRES Committee East of England - Cambridge South).

**10**   **Isolation of primary cholangiocytes**

**11**   Excised bile duct segments were placed in a 10cm plate and washed once

**12**   with William's E medium (Gibco, Life Technologies). A longitudinal incision

**13**   was made along the wall of the excised bile duct segment exposing the lumen

**14**   and 10-15ml of William's E medium were added to cover the tissue. The

**15**   luminal epithelium was subsequently scraped off using a surgical blade, while

**16**   submerged in medium. The supernatant was collected and the tissue and

**17**   plate were washed 2-3 times with William's E medium to harvest any

**18**   remaining cells. The supernatant and washes were centrifuged at 444g for 4

**19**   minutes. The pellet was washed with William's E, re-centrifuged and the

**20**   supernatant was discarded (Figure 1a).

**21**   Excised gallbladders were placed in a 15cm plate, a longitudinal incision was

**22**   made along the wall of the excised gallbladder and the lumen was washed

**23**   once with William's E medium (Gibco, Life Technologies). Cholangiocytes

were isolated and harvested following the method described above (Supplementary Fig. 3a).

For isolation through brushings, an excised bile duct segment was placed in a 10cm plate and cannulated using an ERCP brush. The lumen was brushed 10-20 times and the cells were harvested by washing the brush several times in a falcon tube containing 40-50 ml of William's E medium (Supplementary Fig. 3b).

**Generation and culture of ECOs**

Isolated primary cholangiocytes were centrifuged at 444g for 4 minutes and re-suspended in a mixture of 66% matrigel (BD Biosciences, catalogue number: 356237) and 33% William's E medium (Gibco, Life Technologies) supplemented with 10mM nicotinamide (Sigma-Aldrich), 17mM sodium bicarbonate (Sigma Aldrich), 0.2mM 2-Phospho-L-ascorbic acid trisodium salt (Sigma-Aldrich), 6.3mM sodium pyruvate (Invitrogen), 14mM glucose (Sigma-Aldrich), 20mM HEPES (Invitrogen), ITS+ premix (BD Biosciences), 0.1µM dexamethasone (R&D Systems), 2mM Glutamax (Invitrogen),100U/ml penicillin per 100µg/ml streptomycin, 20ng/ml EGF (R&D Systems), 500ng/ml R-Spondin (R&D Systems) and 100ng/ml DKK-1 (R&D Systems). The cell suspension was plated in 24-well plate format, at 50µl/well, so that a small dome of matrigel was formed in the centre of each well and then incubated at 37$^o$C for 10-30 minutes until it solidified. Subsequently, 1ml of William's E medium with supplements was added. The culture medium was changed every 48 hours.

To split the cells, the matrigel was digested by adding Cell Recovery Solution (Corning) for 30 minutes at 4$^{o}$C. The resulting cell suspension was harvested, centrifuged at 444g for 4 minutes, washed once with William's E medium and re-suspended in 66% matrigel and 33% William's E medium with supplements, as described above.

All experiments were performed using passage 20 ECOs unless otherwise stated.

**Cell line identity**

Demographic data for donor corresponding to the each ECO lines is provided in supplementary table 1. Following derivation ECO lines were authenticated by matching their karyotype (Supplementary Fig. 2c) to the sex of the donor of origin. The lines were tested on a regular basis and found to be negative for mycoplasma contamination.

**Immunofluorescence, RNA extraction and Quantitative Real Time PCR**

IF, RNA extraction and QPCR were performed as previously described (9). A complete list of the primary and secondary antibodies used is provided in supplementary table 3. A complete list of the primers used is provided in supplementary table 4.

All QPCR data are presented as the median, interquartile range (IQR) and range (minimum to maximum) of four independent biological replicates. Values are relative to the housekeeping gene Hydroxymethylbilane Synthase (*HMBS*).

All IF images were acquired using a Zeiss Axiovert 200M inverted microscope or a Zeiss LSM 700 confocal microscope. Imagej 1.48k software (Wayne

17

Rasband, NIHR, USA, http://imagej.nih.gov/ij ) was used for image processing. IF images are representative of at least 3 different experiments. IF images of reconstructed gallbladder sections are representative of 5 different animals.

**Microarrays**

RNA for microarray analysis was collected from 3 different ECO lines (n=3). The RNA was assessed for concentration and quality using a SpectroStar (BMG Labtech, Aylesbury, UK) and a Bioanalyser (Agilent Technologies, Cheadle, UK). Microarray experiments were performed at Cambridge Genomic Services, University of Cambridge, using the HumanHT-12 v4 Expression BeadChip (Illumina, Chesterford, UK) according to the manufacturer's instructions. Briefly, 200ng of Total RNA underwent linear amplification using the Illumina TotalPrep RNA Amplification Kit (Life Technologies, Paisley, UK) following the manufacturer's instructions. The concentration, purity and integrity of the resulting cRNA were measured by SpectroStar and Bioanalyser. Finally cRNA was hybridised to the HumanHT-12 v4 BeadChip overnight followed by washing, staining and scanning using the Bead Array Reader (Illumina). The microarray data are available on ArrayExpress (Accession number: E-MTAB-4591). For reviewer access, please use the following login details Username: Reviewer_E-MTAB-4591 Password: rtIImbi0

**Microarrays analysis**

Raw data was loaded into R using the lumi package from bioconductor (25) and divided into subsets according to the groups being compared; only the samples involved in a given comparison are used. Subsets were then filtered

to remove any non-expressed probes using the detection p-value from Illumina. Across all samples probes for which the intensity values were not statistically significantly different (p>0.01) from the negative controls were removed from the analysis. Following filtering the data was transformed using the Variance Stabilization Transformation (26) from lumi and then normalised to remove technical variation between arrays using quantile normalisation. Comparisons were performed using the limma package (27) with results corrected for multiple testing using False Discovery Rate (FDR) correction. Finally the quality of the data was assessed along with the correlations between samples within groups.

Probes differentially expressed between HEP and ECOs representing the aggregate transcriptional "signature" of ECOs were selected for Euclidean hierarchical clustering using Perseus software (MaxQuant). Standard scores (z-scores) of the log2 normalized probe expression values across the different conditions were calculated and used for this analysis.

**Western Analysis**

Total protein was extracted with lysis buffer (50mM Tris pH 8, 150mM NaCl, 0.1% SDS, 0.5% sodium deoxycholate, 1% Trition X-100 and protease and phosphatase inhibitors). Protein concentrations were determined by BCA Protein Assay Kit (Thermo Fisher Scientific) according to the manufacturer's instructions. Samples were prepared for Western blot by adding 1x NuPAGE LDS Sample Buffer with 1% β-mercaptoethanol and incubated for 5 minutes at 95°C. Protein (25 µg) was separated by 4-12% NuPAGE Bis-Tris protein gels (Invitrogen) and transferred onto PVDF membranes (Bio-Rad). Proteins were detected by probing with antibodies specific to Phospho-β-catenin

(Ser33/37/Thr41) (Cell Signalling Technology), Active-β-catenin (Millipore), Total-β-catenin (R&D), α-tubulin (Sigma) followed by incubation with horseradish peroxidase anti-mouse, anti-goat or anti-rabbit secondary antibodies. Membranes were developed using Pierce ECL Western blotting substrate (Thermo Scientific) according to the manufacturer's instructions.

**Rho Kinase activity analyses**

Rho Kinase activity was measured using a commercially available kit (Cell Biolabs, STA-416) according to the manufacturer's instructions

**Flow cytometry analyses**

ECO organoids were harvested using Cell Recovery Solution (Corning) for 30 minutes at 4$^o$C, centrifuged at 444g for 4 minutes and dissociated to single cells using TrypLE$^{TM}$ Express (Gibco). The cells were subsequently fixed using 4% PFA for 20 minutes at 4$^o$C. Cell staining and flow cytometry analyses were performed as previously described (9,28).

**Karyotyping**

ECO organoids were harvested using Cell Recovery Solution (Corning), dissociated to single cells as described above, plated in gelatin coated plates and cultured using William's E medium with supplements. When the cells were sub-confluent, usually after 72hrs, the cultures were incubated for 3-4 hours with William's E medium with supplements containing 0.1µg/ml colcemid (Karyomax®, Gibco). The cells were then harvested using Trypsin-EDTA (0.05%) (Gibco) for 4-5 minutes at 37$^o$C, centrifuged at 344g for 5 minutes and re-suspended in 5mls of KCl hypotonic solution (0.055M). The suspension was re-centrifuged at 344g for 5 minutes, 2 mls of a 3:1 100%

methanol:glacial acetic acid solution were added and slides were prepared as previously described (29)

**Comparative Genomic Hybridization analyses**

Genomic DNA was labeled using the BioPrime DNA Labeling Kit (Invitrogen), according to the manufacturer's instructions and samples were hybridised to Agilent Sureprint G3 unrestricted CGH ISCA 8x60K human genome arrays following the manufacturer's protocol, as previously described (30). The data was analysed using the Agilent CytoGenomics Software.

**Rhodamine123 transport assay**

The Rhodamine 123 transport assay was performed as previously described (9) and images were acquired using a Zeiss LSM 700 confocal microscope. Fluorescence intensity was measured between the organoid interior and exterior and luminal fluorescence was normalized over the background of the extraluminal space. Each experiment was repeated in triplicate. Error bars represent SD. Mean fluorescence intensity comparisons were performed using a two sided student's t-test.

**Cholyl-Lysyl-Fluorescein transport assay**

To achieve loading with Cholyl-Lysyl-Fluorescein (CLF, Corning Incorporated), ECO organoids were split in 5µM of CLF and incubated at $37^{o}$C for 30 minutes. Images were acquired using a Zeiss LSM 700 confocal microscope and fluorescence intensity was measured between the organoid interior and exterior as described for the Rhodamine 123 transport assay. To demonstrate that the changes in CLF fluorescence intensity observed were secondary to active export of CLF from the organoid lumen, the experiment was repeated with 5µM of unconjugated Fluorescein Isothiocyanate (FITC)

(Sigma-Aldrich) as a control. Fluorescence intensity measurements were performed as described for the Rhodamine 123 transport assay. Each experiment was repeated in triplicate. Error bars represent SD. Mean fluorescence intensity comparisons were performed using a two sided student's t-test.

**GGT activity**

GGT activity was measured in triplicate using the MaxDiscovery™ gamma-Glutamyl Transferase (GGT) Enzymatic Assay Kit (Bioo scientific) based on the manufacturer's instructions. Error bars represent SD. Mean absorbance was compared using a two sided student's t-test.

**Alkaline Phosphatase staining**

Alkaline phosphatase was carried out using the BCIP/NBT Color Development Substrate (5-bromo-4-chloro-3-indolyl-phosphate/nitro blue tetrazolium) (Promega) according to the manufacturer's instructions.

**Response to Secretin and Somatostatin**

Responses to secretin and somatostatin were assessed as previously described (9).

**Generation of ECOs expressing Green Fluorescent Protein**

EGFP expressing VSV-G pseudotyped, recombinant HIV-1 lentiviral particles were produced with an optimized second generation packaging system by transient co-transfection of three plasmids into HEK 293T cells (ATCC CRL-11268). EGFP expression is under control of a core EF1α-promoter. All plasmids were a gift from Didier Trono and obtained from addgene (pWPT-GFP #12255, psPAX2 #12260, pMD2.G, #12259). Viral infection of organoids was performed as previously described (31). Infected ECOs were expanded

for 2 passages, harvested as described above for flow cytometry analyses and cell sorting by flow cytometry for GFP positive cells was performed. GFP expressing single cells were plated using our standard plating method and cultured in William's E medium with supplements for 1-2 weeks until fully grown ECO organoids developed.

**Generation of ECO populated PGA scaffolds**

1mm thick PolyGlycolic Acid (PGA) scaffolds with a density of 50mg/cc were used for all experiments. Prior to seeding cells, the PGA scaffolds were pre-treated with a 1M NaOH for 10-30 seconds washed 3 times, decontaminated in a 70% ethanol solution for 30 minutes and then air-dried for another 30 minutes until all the ethanol had fully evaporated. All scaffolds were a gift from Dr Sanjay Sinha and obtained from Biomedical Structures (Biofelt).

ECOs were harvested and dissociated to single cells as previously described for flow cytometry analyses. $5\text{-}10\text{x}10^6$ cells were re-suspended in 100 µl of William's E medium with supplements, seeded on a scaffold surface area of $1\text{cm}^2$ and incubated at $37^\text{o}\text{C}$ for 30-60 minutes to allow the cells to attach to the scaffold. The scaffolds were placed in wells of a 24-well plate and checked at regular intervals during this period to ensure the medium did not evaporate. If necessary, 10-20 µl of William's E medium with supplements were added. After 1 hour, 2-3 mls of William's E medium with supplements were added to the wells and the medium was changed twice weekly.

**Generation of densified collagen tubes**

Densified collagen tubes were prepared using a novel approach. A 3D printed chamber was fabricated, consisting of a funnel piece and a base plate. A 250µm thick metallic wire was mounted into the base plate and fed through

the centre of the funnel. Absorbent paper towels were compacted between the two 3D printed parts, which were then screwed together. 5 mg mL$^{-1}$ collagen gel solution, loaded with cells, was poured into the funnel and gelled at 37ºC for 30 min. After that time, the screws were loosened and, by placing the 3D printed chambers at 37ºC for 2-4h, water was drawn out of the collagen gel. A cell-loaded densified collagen tube was thus formed with a 250µm lumen and a wall thickness of 30-100 µm, determined by the duration of the drying phase. Upon removal from the chamber, the tube was trimmed for excess collagen and cut to the required length.

**Culture of Human Mammary Epithelial Cells (HMECs)**

HMECs and the required tissue culture consumables were purchased as a kit from Lonza (cat no. cat no. CC-2551B) and the cells were cultured according to the supplier's instructions

**Animal experiments**

All animal experiments were performed in accordance with UK Home Office regulations. Immunodeficient NOD.Cg-Prkdc$^{scid}$ Il2rg$^{tm1Wjl}$/SzJ (NSG) mice which lack B, T and NK lymphocytes (32) were bred in-house with food and water available ad libitum pre- and post-procedures. A mix of male and female animals were used, aged approximately 6-8 weeks. All the ECO-constructs used were populated with ECOs derived from the common bile duct.

**Generation of ExtraHepatic Biliary Injury mouse model**

To generate a model of extrahepatic biliary injury, midline laparotomy was performed and the gallbladder was first mobilized by dividing the ligamentous attachment connecting its fundus to the anterior abdominal wall under isoflurane general anesthesia. A longitudinal incision was then made along

2/3 of the length of the gallbladder, from the fundus towards Hartmann's pouch (neck of gallbladder).

**Biliary reconstruction in EHBI mice**

To reconstruct the gallbladder, a scaffold section measuring approximately 1 x 1 mm (seeded with ECOs or without ECOs in controls) was sutured as a 'patch' to close the defect using 4 – 6 interrupted 10'0 non-absorbable nylon sutures under 40x magnification. The laparotomy was closed in two layers with continuous 5'0 absorbable Vicryl sutures. The animals were given buprenorphine (temgesic 0.1 mg/kg) analgesia as a bolus and observed every 15 minutes in individual cages until fully recovered.

8 animals underwent biliary reconstruction using an ECO-populated scaffold. All animals survived up to 104 days without complications and were culled electively for further analyses. Two control experiments were performed, where the animals underwent biliary reconstruction using acellular scaffolds. Both animals died within 24 hours from bile leak, therefore no further control experiments were performed to minimize animal discomfort.

**Bile duct replacement**

The native common bile duct was divided and a short segment excised. The populated densified collagen tube was anastomosed end-to-end, using interrupted 10'0 nylon sutures, between the divided proximal and distal common bile duct. A length of 5'0 nylon suture material (diameter 100 µm) was inserted into the collagen tube and fed into the proximal and distal common bile duct to ensure patency of the lumen during the anastomosis. After the anastomosis was complete, the 5'0 suture was pushed into the duodenum through the distal bile duct and was removed through an incision in

the duodenum, which was then closed with interrupted 10'0 nylon sutures. Lumen patency was assessed at the time of transplantation through light microscopy and cannulation of the lumen with a 5'0 non-absorbable suture. Transplantation was abandoned as futile in case of fully occluded tubes due to cell infiltration. These events were considered construct/tube failure rather than surgical complications and therefore were not censored in the survival analysis.

**Bile duct ligation**

C57BL/6 mice were purchased from The Jackson Laboratory (Bar Harbor, ME). The mice were housed and bred in a Minimal Disease Unit at the animal facility at Oslo University Hospital, Rikshospitalet, Oslo. All experiments were performed on male mice between 8 and 12 weeks of age. We performed a median laparotomy exposed the bile duct and ligated the common bile duct close to the junction of the hepatic bile ducts. Sham operated mice underwent the exact same procedure without ligation. Serum was harvested after 5 days. Alanine transaminase (ALT), aspartate transaminase (AST) and alkaline phosphatase (ALP) were measured in serum using an ADVIA 1800 (Siemens) at The Central Laboratory, Norwegian School of Veterinary Science. All animal experiments were approved by the Norwegian Food Safety Authority (project license no FOTS 8210/15) and all animals received human care in line with "Guide for the Care and Use of Laboratory Animals" (National Institutes of Health Publication, 8th Edition, 2011).

**Blood sample collection**

**Light microscopy imaging**

Light microscopy images of excised reconstructed gallbladders were acquired using a Leica MZFLIII fluorescence dissecting microscope. The images are representative of 5 animals.

**Cryosectioning and Histology**

Excised gallbladders were fixed in 4% PFA, immersed in sucrose solution overnight, mounted in optimal cutting temperature (OCT) compound and stored at -80°C until sectioning. Sections were cut to a thickness of 10µm using a cryostat microtome and mounted on microscopy slides for further analysis

**Haematoxylin and Eosin Staining**

H&E staining was performed using Sigma-Aldrich reagents according to the manufacturer's instructions. Briefly, tissue sections were hydrated, treated with Meyer's Haematoxylin solution for 5 minutes (Sigma-Aldrich), washed with warm tap water for 15 minutes, placed in distilled water for 30-60 seconds and treated with eosin solution (Sigma-Aldrich) for 30-60 seconds.

The sections were subsequently dehydrated and mounted using the Eukitt® quick-hardening mounting medium (Sigma-Aldrich). Histology sections were reviewed by an independent histopathologist with a special interest in hepatobiliary histology (SD).

**TUNEL assay**

The TUNEL assay was performed using a commercially available kit (abcam, ab66110) according to the manufacturer's instructions.

**Fluorescein Isothiocyanate (FITC) cholangiogram**

In situ FITC cholangiogram was performed in sacrificed animals after dissection of the gallbladder free from the adherent liver lobes, but before surgical interruption of the extrahepatic biliary tree. The distal bile duct was cannulated with a 23½ gauge needle and FITC injected retrogradely into the gallbladder and images taken under a fluorescent microscope.

**Magnetic resonance cholangiogram (MRCP)**

Magnetic resonance cholangiogram (MRCP) was performed after sacrifice of the animals. MRCP was performed at 4.7T using a Bruker BioSpec 47/40 system. A rapid acquisition with relaxation enhancement sequence was used with an echo train length of 40 echoes at 9.5ms intervals, a repetition time of 1000ms, field of view $5.84\times4.18\times4.18cm^3$ with a matrix of 256×180×180 yielding an isotropic resolution of 230µm. The actively-decoupled four-channel mouse cardiac array provided by Bruker was used for imaging.

For the second mouse imaged, for higher signal to noise ratio to give improved visualisation of the biliary ducts a two-dimensional sequence was used with slightly varied parameters (24 spaced echoes at 11ms intervals to give an effective echo time of 110ms; repetition time 5741ms; matrix size of

256×256; field of view of 4.33×5.35cm$^2$ yielding a planar resolution of 170×200µm$^2$). Fifteen slices were acquired coronally through the liver and gall bladder with a thickness of 0.6mm. For this acquisition, a volume coil was used to reduce the impact of radiofrequency inhomogeneity.

To examine the biliary ducts and gall bladder, images were prepared by maximum intensity projections. Structural imaging to rule out neoplastic growths was performed using a T1-weighted 3D FLASH (fast low-angle shot) sequence with a flip angle of 25°, repetition time of 14ms and an echo time of 7ms. The matrix was 512×256×256 with a field of view of 5.12×2.56×2.56cm$^3$ for a final isotropic resolution of 100µm.

The MRCP images were reviewed by 2 independent radiologists with a special interest in hepatobiliary radiology (EMG, SU).

**Statistical analyses**

All statistical analyses were performed using GraphPad Prism 6. For small sample sizes where descriptive statistics are not appropriate, individual data points were plotted. For comparison between 2 mean values a 2-sided student's t-test was used to calculate statistical significance. The normal distribution of our values was confirmed using the D'Agostino & Pearson omnibus normality test where appropriate. Variance between samples was tested using the Brown-Forsythe test. For comparing multiple groups to a reference group one-way ANOVA with Dunnett correction for multiple comparisons was used between groups with equal variance, while the Kruskal-Wallis test with Dunn's correction for multiple comparisons was applied for groups with unequal variance. Survival was compared using log-rank (Mantel-Cox) tests. Where the number of replicates (n) is given this

refers to biological replicates or number of different animals unless otherwise stated.

For animal experiments, initial group sizes were estimated based on previous study variance. No statistical methods were used to calculate sample size. No formal randomization method was used to assign animals to the experimental group. However; animals were randomly picked from a cage by a technician not involved in the study. No animals were excluded from the analysis. No blinding was used when reviewing radiology images or histopathology slides.

**Author Contributions:** FS: Design and concept of study, execution of experiments and data acquisition, development of protocols and validation, collection and interpretation of data, production of figures, manuscript writing, editing and final approval of manuscript; AWJ: Conception of the technique, scaffold design and generation of densified collagen tubular scaffolds; OCT: animal experiments including kidney capsule injections; cell culture, provision and harvesting of mouse tissue; StS: Magnetic Resonance Imaging (MRI); EMG, SSU: MRI review and reporting; RLG: Animal experiments, IF, tissue histology; MCDB: Cell culture, generation of viral particles, viral transduction, generation of GMP-ECOs; NLB, LV: Animal experiments; MJGV, PM: Bioinformatics analyses; DO: Flow cytometry analyses; LY: Western blot analyses; AB: Flow cytometry analyses, bioinformatics support; JB: Tissue histology, IF; MarZ: Scaffold preparation; MTP: Generation of viral particles, viral transduction, generation of GMP-ECOs; MP: Generation of viral particles; GMS: scaffold generation; PMM,KES: maintenance and provision of fibroblast controls; NP: tissue culture; NG, CAR: Harvesting and preparation of primary

tissue; IS: Karyotyping, CGH analyses; SD: Histology review and reporting; WS, JC, KBJ, MatZ, SaS, WTHG, GJA, NRFH, SEB, TW, THK, EM: critical revision of the manuscript for important intellectual content. AEM: Scaffold design, critical revision of the manuscript for important intellectual content. KSP: Primary tissue provision, animal experiments, design and concept of study, study supervision, interpretation of data, editing and final approval of manuscript. LV: Design and concept of study, study supervision, interpretation of data, editing and final approval of manuscript.

**Competing interests:** LV is a founder and shareholder of DefiniGEN. The remaining authors have nothing to disclose.

**References**

1. Murray, K. F. & Carithers, R. L. AASLD practice guidelines: Evaluation of the patient for liver transplantation. *Hepatology* **41,** 1407–1432 (2005).

2. Perkins, J. D. Are we reporting the same thing?: Comments. *Liver Transplant.* **13,** 465–466 (2007).

3. Skaro, A. I. *et al.* The impact of ischemic cholangiopathy in liver transplantation using donors after cardiac death: The untold story. *Surgery* **146,** 543–553 (2009).

4. Enestvedt, C. K. *et al.* Biliary complications adversely affect patient and graft survival after liver retransplantation. *Liver Transpl.* **19,** 965–72 (2013).

5. Gallo, A. & Esquivel, C. O. Current options for management of biliary atresia. *Pediatr. Transplant.* **17,** 95–98 (2013).

6. Felder, S. I. *et al.* Hepaticojejunostomy using short-limb Roux-en-Y reconstruction. *JAMA Surg* **148,** 253–7-8 (2013).

7. Sampaziotis, F., Segeritz, C.-P. & Vallier, L. Potential of human induced pluripotent stem cells in studies of liver disease. *Hepatology* **62,** 303–311 (2015).

8. Kanno, N., LeSage, G., Glaser, S., Alvaro, D. & Alpini, G. Functional heterogeneity of the intrahepatic biliary epithelium. *Hepatology* **31,** 555–61 (2000).

9. Sampaziotis, F. *et al.* Cholangiocytes derived from human induced

pluripotent stem cells for disease modeling and drug validation. *Nat. Biotechnol.* 1–11 (2015). doi:10.1038/nbt.3275

10. LeSage, G., Glaser, S. & Alpini, G. Regulation of cholangiocyte proliferation. *Liver* **21,** 73–80 (2001).

11. Huch, M. *et al.* Long-Term Culture of Genome-Stable Bipotent Stem Cells from Adult Human Liver. *Cell* **160,** 299–312 (2014).

12. Masyuk, A. I., Masyuk, T. V & LaRusso, N. F. Cholangiocyte primary cilia in liver health and disease. *Dev. Dyn.* **237,** 2007–12 (2008).

13. Tabibian, J. H., Masyuk, A. I., Masyuk, T. V., O'Hara, S. P. & LaRusso, N. F. Physiology of cholangiocytes. *Compr. Physiol.* **3,** 541–565 (2013).

14. Cízková, D., Morký, J., Micuda, S., Osterreicher, J. & Martínková, J. Expression of MRP2 and MDR1 transporters and other hepatic markers in rat and human liver and in WRL 68 cell line. *Physiol. Res.* **54,** 419–28 (2005).

15. Gigliozzi, A. *et al.* Molecular identification and functional characterization of Mdr1a in rat cholangiocytes. *Gastroenterology* **119,** 1113–22 (2000).

16. Xia, X., Francis, H., Glaser, S., Alpini, G. & LeSage, G. Bile acid interactions with cholangiocytes. *World J. Gastroenterol.* **12,** 3553–63 (2006).

17. Caperna, T. J., Blomberg, L. A., Garrett, W. M. & Talbot, N. C. Culture of porcine hepatocytes or bile duct epithelial cells by inductive serum-free media. *In Vitro Cell. Dev. Biol. Anim.* **47,** 218–33 (2011).

18. Marinelli, R. A. *et al.* Secretin induces the apical insertion of aquaporin-1 water channels in rat cholangiocytes. *Am. J. Physiol.* **276,** G280-6 (1999).

19. Gong, A.-Y. *et al.* Somatostatin stimulates ductal bile absorption and inhibits ductal bile secretion in mice via SSTR2 on cholangiocytes. *Am. J. Physiol. Cell Physiol.* **284,** C1205-14 (2003).

20. Ito, M. *et al.* NOD/SCID/gamma(c)(null) mouse: an excellent recipient mouse model for engraftment of human cells. *Blood* **100,** 3175–82 (2002).

21. Jabłonska, B. End-to-end ductal anastomosis in biliary reconstruction: indications and limitations. *Can. J. Surg.* **57,** 271–277 (2014).

22. Gjorevski, N. *et al.* Designer matrices for intestinal stem cell and organoid culture. *Nature* **539,** 560–564 (2016).

23. Koo, B. K. & Clevers, H. Stem cells marked by the r-spondin receptor LGR5. *Gastroenterology* **147,** 289–302 (2014).

24. Farin, H. F., Van Es, J. H. & Clevers, H. Redundant sources of Wnt regulate intestinal stem cells and promote formation of paneth cells. *Gastroenterology* **143,** 1518–1529.e7 (2012).

25. Du, P., Kibbe, W. a & Lin, S. M. lumi: a pipeline for processing Illumina microarray. *Bioinformatics* **24,** 1547–8 (2008).

26. Lin, S. M., Du, P., Huber, W. & Kibbe, W. A. Model-based variance-stabilizing transformation for Illumina microarray data. *Nucleic Acids Res.* **36,** (2008).

1 27. Smyth, G. K. Linear models and empirical bayes methods for assessing

2    differential expression in microarray experiments. *Stat Appl Genet Mol*

3    *Biol* **3,** Article3-Article3 (2004).

4 28. Bertero, A. *et al.* Activin/Nodal signaling and NANOG orchestrate

5    human embryonic stem cell fate decisions by controlling the H3K4me3

6    chromatin mark. *Genes Dev.* **29,** 702–17 (2015).

7 29. Campos, P. B., Sartore, R. C., Abdalla, S. N. & Rehen, S. K.

8    Chromosomal spread preparation of human embryonic stem cells for

9    karyotyping. *J. Vis. Exp.* 4–7 (2009). doi:10.3791/1512

10 30. Hannan, N. R. F. *et al.* Generation of multipotent foregut stem cells from

11    human pluripotent stem cells. *Stem Cell Reports* **1,** 293–306 (2013).

12 31. Koo, B.-K., Sasselli, V. & Clevers, H. Retroviral gene expression control

13    in primary organoid cultures. *Curr. Protoc. Stem Cell Biol.* **27,** Unit 5A.6.

14    (2013).

15 32. Shultz, L. D. *et al.* Human lymphoid and myeloid cell development in

16    NOD/LtSz-scid IL2R gamma null mice engrafted with mobilized human

17    hemopoietic stem cells. *J. Immunol.* **174,** 6477–6489 (2005).

18

19

**Figure Legends**

**Figure 1**

4  Derivation and characterization of Extrahepatic Cholangiocyte Organoids

5  (ECOs). **(a)** Schematic representation of the method used for the derivation of

6  ECOs. **(b)** Photograph of a 24-well plate well containing ECO organoids under

7  3D culture conditions. Scale bar: 1cm **(c)** Light microscopy image of ECO

8  organoids. Scale bar: 1 mm **(d)** Transmitted electron microscopy picture of

9  ECOs demonstrating the presence of cilia (black arrowhead). Scale bar:

10  500nm **(e)** Quantitative real time PCR (QPCR) confirming the expression of

11  biliary markers in Passage 1 (P1), Passage 10 (P10) and Passage 20 (P20)

12  ECOs compared to freshly isolated Primary Cholangiocytes (PCs) and

13  Embryonic Stem  (ES) cells used as a negative control, n=4 biological

14  replicates. Center line, median; box, interquartile range (IQR); whiskers, range

15  (minimum to maximum). Values are relative to the housekeeping gene

16  Hydroxymethylbilane Synthase (*HMBS*) **(f)** Immunofluorescence (IF) analyses

17  confirming the expression of biliary markers in ECO organoids. Scale bars:

18  100 μm. Single channel and higher magnification images are provided in

19  Supplementary Figure 6a. **(g)** Euclidian hierarchical clustering analysis

20  comparing the transcriptome of primary cholangiocytes (Primary), passage 20

21  ECOs (ECO), iPS-derived intrahepatic cholancgiocyte-like-cells (iChoLC), ES

22  cells (ES) and hepatocytes (HEP). For each probe, standard scores (z-

23  scores) indicate the differential expression measured in number of standard

24  deviations from the average level across all the samples. Clusters of genes

1  expressed in ECOs, primary cholangiocytes or both cell types are indicated.

2  GO analyses for each cluster are provided in Supplementary Figure 7e. The

3  data corresponds to biological triplicates.

4

5  **Figure 2**

6  Functional characterization of ECO organoids. **(a)** Fluorescence images

7  demonstrating secretion of the MDR1 fluorescent substrate rhodamine 123 in

8  the lumen of ECOs. Luminal accumulation of rhodamine is inhibited the MDR1

9  inhibitor verapamil, confirming MDR1 activity. Scale bars: 100 µm. **(b)**

10  Fluorescence intensity along the red line in **(a)**. **(c)** Mean intraluminal

11  fluorescence intensity normalized to background in freshly plated Primary

12  Cholangiocytes (Rho PCs), Passage 20 ECOs (Rho P20) and P20 ECOs

13  treated with verapamil (Ver). Error bars, Standard Deviation (SD); n=1565

14  measurements in total. Asterisks (****) indicate statistical significance

15  (*P*<0.001, Kruskal-Wallis test with Dunn's correction for multiple comparisons)

16  **(d)** Luminal extrusion of the fluorescent bile acid CLF compared to controls

17  loaded with Fluorescein Isothiocyanate (FITC), confirming active bile acid

18  transfer. Scale bars: 100 µm. **(e)** Fluorescence intensity along the red line in

19  **(d)**. **(f)** Mean intra-luminal fluorescence intensity normalized over background,

20  n=1947 total measurements. Error bars, SD; asterisks as in **(c)**. **(g)** ALP

21  staining of ECOs. Scale bars: Light microscopy: 500µm, Whole well images:

22  1cm. **(h)** Mean GGT activity of P20 ECOs vs. PCs; error bars, SD; n=3,

23  asterisks as in **(c)**. **(i,j)** Mean diameter measurements **(i)** and live images **(j)**

24  of ECOs treated with secretin or secretin and somatostatin, n=8. Error bars,

SD; ***$P<0.001$; #$P>0.05$ (Kruskal-Wallis test with Dunn's correction for multiple comparisons). **(a-j)** Data representative of 3 different experiments.

**Figure 3**
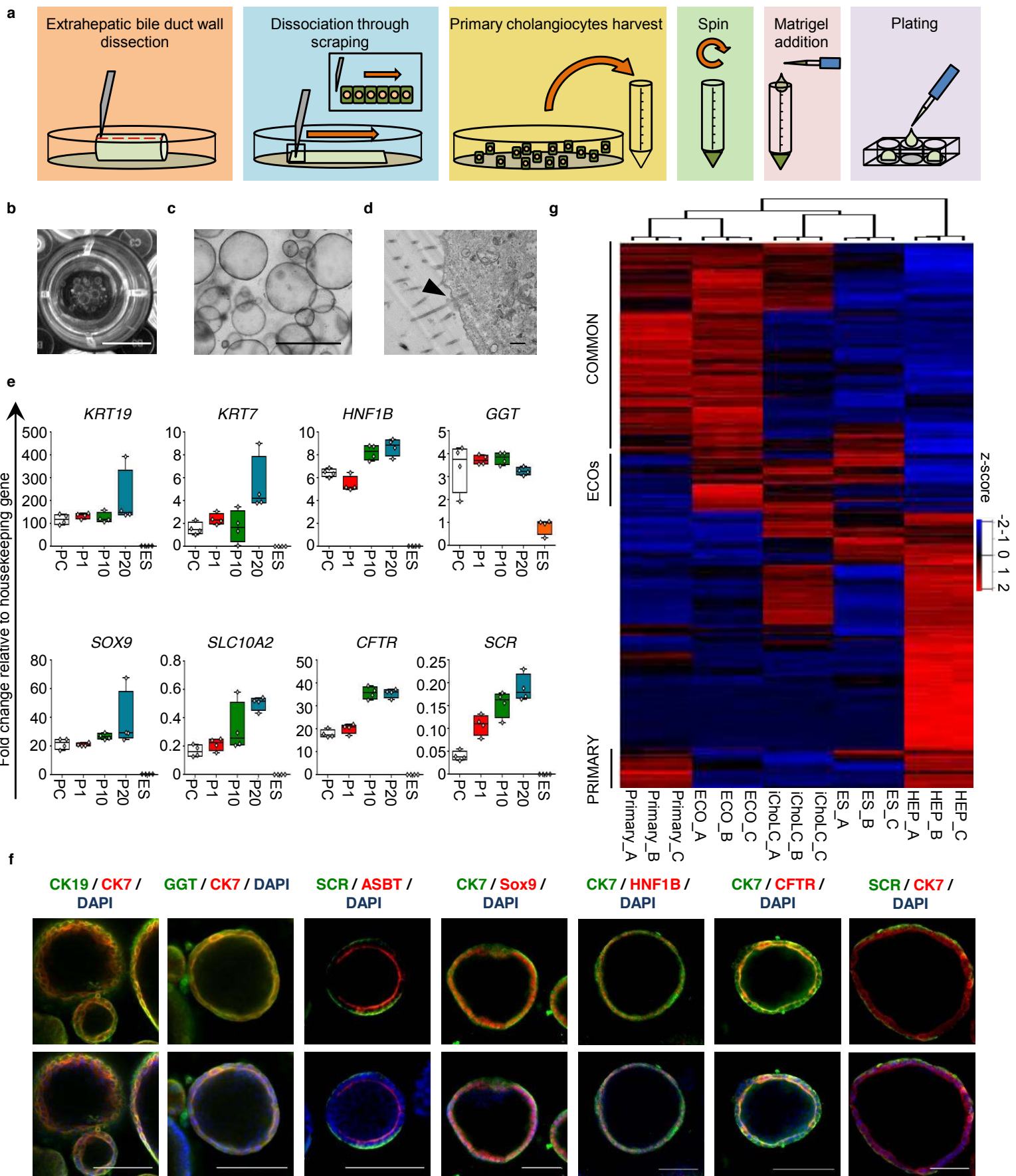
Biliary reconstruction in an extrahepatic biliary injury (EHBI) mouse model using ECOs. **(a)** Schematic representation of the method used for biliary reconstruction. **(b)** Kaplan–Meier survival analysis, demonstrating rescue of EHBI mice following biliary reconstruction with ECO-populated scaffolds. **$P<0.01$ (log-rank test). **(c)** Images of gallbladders reconstructed with acellular PGA scaffolds (scaffold only), PGA scaffolds populated with ECOs (transplanted) and native not reconstructed gallbladder controls (not transplanted), demonstrating full reconstruction with ECO populated scaffolds. CD: cystic duct, CBD: common bile duct, CHD: common hepatic duct, F: fundus, A: anterior surface, P: posterior surface. Scale bars: 500µm. **(d)** H&E staining demonstrating physiological architecture of the reconstructed gallbladders. L: lumen. Scale bars: 100µm **(e)** IF analyses demonstrating the presence of GFP-positive ECOs expressing biliary markers in the reconstructed gallbladders. L: lumen Scale bars: 100 µm. Higher magnification images are provided in supplementary figure 14 **(f,g)** FITC cholangiogram (n=1) **(f)** and Magnetic Resonance Cholangio-Pancreatography (MRCP) images (n=2) **(g)** of reconstructed (transplanted) vs. native control (not transplanted) gallbladders (GB) demonstrating a patent lumen and unobstructed communication with the rest of the biliary tree. Scale bars: 1mm
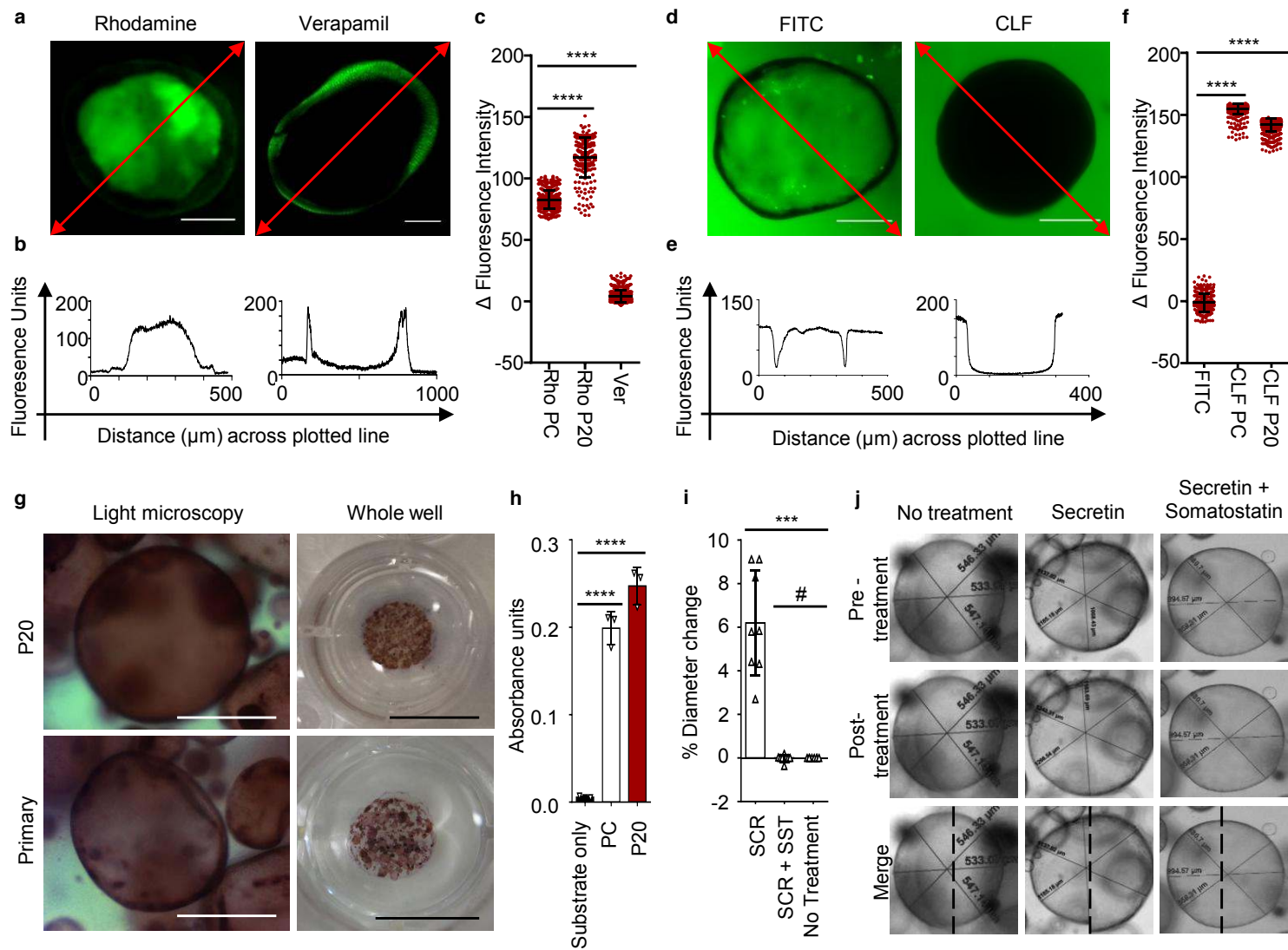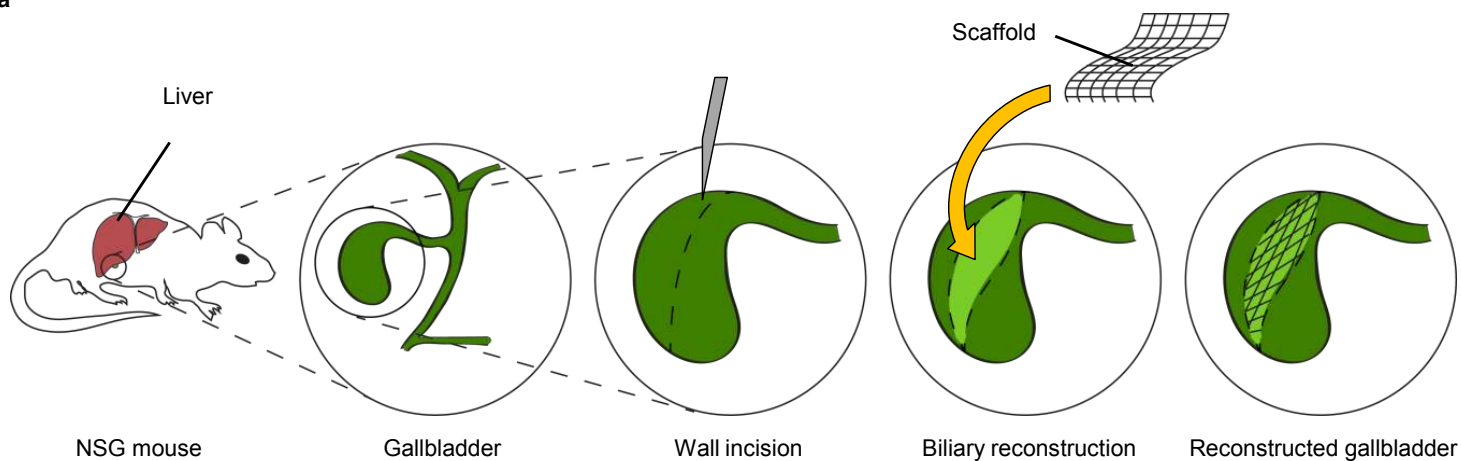
**Figure 4**

Bile duct replacement using ECO-populated densified collagen tubes. **(a)** Schematic representation of the method used. **(b)** Postmortem images of mice receiving ECO-populated collagen tubes (ECOs) vs. mice receiving fibroblast-populated tubes (fibroblasts). Bile flow results in yellow pigmentation of ECO-tubes. The white color of the fibroblast conduit combined with a dilated bile-filled (yellow color) proximal bile duct (PDB) suggests luminal occlusion, resulting in bile leak (yellow peritoneal pigmentation; white dashed line). SC: Collagen tubes/scaffolds; DBD: Distal Bile duct; scale bars 500μm. **(c)** Images of a thin walled construct resembling the native bile duct in animals receiving ECO-populated tubes vs. a thickened construct with no distinguishable lumen in animals receiving fibroblast tubes. Scale bars 500μm. **(d)** QPCR using human-specific primers confirming the expression of biliary markers by transplanted ECO-populated tubes (ECOs in vivo) compared to cultured ECOs (ECOs in vitro) and mouse biliary tissue used as a negative control, n=4 replicates. Center line, median; box, interquartile range (IQR); whiskers, range (minimum to maximum). Values are relative to *HMBS* expression. **(e)** H&E staining demonstrating the presence of a biliary epithelium and a patent lumen in ECO-tubes but not fibroblast constructs. Scale bars 100μm. **(f)** IF analyses demonstrating a GFP+/ CK19+ epithelium lining the lumen of ECO-constructs, vs. obliteration of the lumen by fibroblasts in fibroblast constructs. Scale bars 100μm. **(g)** FITC cholangiogram, demonstrating lumen patency in ECO-tubes vs. lumen

1    occlusion in fibro-constructs. Scale bars: 500μm **(h)** ALP activity is observed

2    only in ECO-tubes, but not in fibroblast constructs. Scale bars: 500μm

**Sampaziotis et al. Figure 1**

**a**

| Extrahepatic bile duct wall dissection | Dissociation through scraping | Primary cholangiocytes harvest | Spin | Matrigel addition | Plating |

**b**    **c**    **d**    **g**

**e**

*KRT19*   *KRT7*   *HNF1B*   *GGT*

Fold change relative to housekeeping gene

*SOX9*   *SLC10A2*   *CFTR*   *SCR*

**g**

COMMON

ECOs

PRIMARY

z-score

-2 -1 0 1 2

Primary_A Primary_B Primary_C ECO_A ECO_B ECO_C iChoLC_A iChoLC_B iChoLC_C ES_A ES_B ES_C HEP_A HEP_B HEP_C

**f**

CK19 / CK7 / DAPI   GGT / CK7 / DAPI   SCR / ASBT / DAPI   CK7 / Sox9 / DAPI   CK7 / HNF1B / DAPI   CK7 / CFTR / DAPI   SCR / CK7 / DAPI

**a** Rhodamine   Verapamil

**b** Fluorescence Units — Distance (μm) across plotted line

**c** Δ Fluoresence Intensity — Rho PC, Rho P20, Ver

**d** FITC   CLF

**e** Fluorescence Units — Distance (μm) across plotted line

**f** Δ Fluoresence Intensity — FITC, CLF PC, CLF P20

**g** Light microscopy   Whole well — P20, Primary

**h** Absorbance units — Substrate only, PC, P20

**i** % Diameter change — SCR, SCR + SST, No Treatment

**j** No treatment, Secretin, Secretin + Somatostatin — Pre-treatment, Post-treatment, Merge

**Sampaziotis et al. Figure 3**

**a**



NSG mouse | Gallbladder | Wall incision | Biliary reconstruction | Reconstructed gallbladder

**b**

**Survival curve**



| Number of mice at risk | | | | | |
|---|---|---|---|---|---|
| Days | 0 | 1 | 17 | 22 | 75 | 104 |
| Control | 2 | 2 | 0 | 0 | 0 | 0 |
| Scaffold | 8 | 8 | 8 | 5 | 4 | 3 |

**c**



**d**



**e**

GFP | CK19 | GFP / CK19 | GFP / CK19 / DAPI



**f**

Brightfield | FITC | Merge



**g**

Not transplanted | Transplanted

**a**

**b**
ECOs
PBD
L
SC
DBD

Fibroblasts
PBD
SC
DBD

**c**
ECOs
PBD
SC
DBD

Fibroblasts
SC
DBD
PBD

**d**
Fold change relative to housekeeping gene

CK19
CK7
HNF1B
CFTR
SOX9

☐ ECOs in vitro
🟥 ECOs in vivo
⬛ Mouse

**e**
H&E
ECOs
Fibroblasts

**f**
GFP    CK19    GFP / CK19    GFP / CK19 / DAPI

CK19    S100A4    CK19 / S100A4    CK19 / S100A4 / DAPI

**g**
Brightfield    FITC    Merge
ECOs
Fibroblasts

**h**
Unstained    ALP
ECOs
PBD
SC
DBD
DBD
SC
PBD

Fibroblasts
PBD
SC
DBD
DBD
SC
PBD
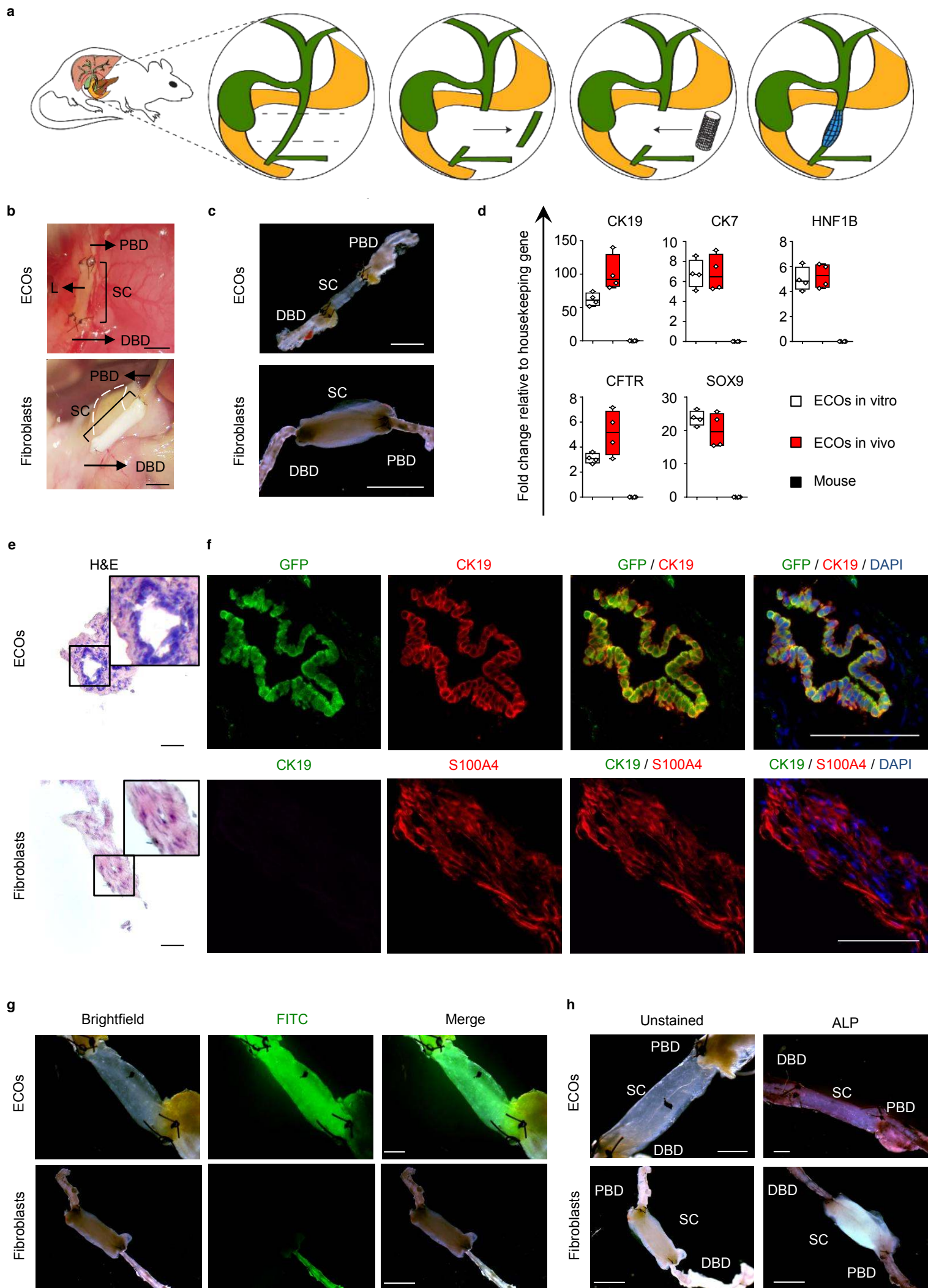
**Supplementary Note**

**Supplementary Results**

To assess the potential of ECOs for tissue engineering, we first interrogated their capacity for populating Polyglycolic Acid (PGA) biodegradable scaffolds commonly used to provide the structural and mechanical support required for tissue reconstruction (1). Indeed, PGA is one of the most widely used synthetic polymers since it does not induce inflammatory responses in the surrounding tissue; it is biodegradable; and it is more flexible and easier to process compared to natural polymers such as collagen (2). To facilitate tracking of the cells, ECOs expressing Green Fluorescent Protein (GFP) were generated through viral transduction (Supplementary Fig. 10a-10b). The resulting cells were seeded on PGA scaffolds, attached to the PGA fibers after 24-48 hours and continued to grow for 4 weeks until the scaffold was confluent (Supplementary Fig 11a-11d). Primary cholangiocytes plated in 2D conditions demonstrated limited expansion potential and failed to reach confluency when seeded on the scaffolds (Supplementary Fig 12a-b), suggesting that the proliferative capacity of ECOs is crucial for successful scaffold colonization. The populated PGA scaffolds (Supplementary Fig 11b-11c), could easily be handled with forceps and divided into smaller pieces with a surgical blade. Furthermore, the cells populating the scaffolds retained expression of biliary markers such as CK7 and CK19 (Supplementary Fig 11e-11f), demonstrated no evidence of EMT (Supplementary Fig. 11e, 11g) and maintained their functional properties including ALP and GGT activity (Supplementary Figure 11h-11i). Therefore, ECOs can successfully populate PGA scaffolds, while maintaining their functionality and marker expression.

We then focused on the generation of a tubular ECO-populated scaffold, which could be used in the context of bile duct replacement surgery. The internal diameter of the mouse CBD is approximately 100μm with a wall thickness of less than 50μm, which precluded the use of a PGA scaffold due to mechanical properties. Instead, we generated densified collagen tubular scaffolds (Supplementary Fig 15a-15b) which were populated with GFP-expressing ECOs (supplementary Fig 15c-15e). The use of densified collagen enabled the generation of constructs with an external diameter ranging from 250 to 600μm and adequate strength to maintain a patent lumen (Supplementary Fig 15d). Importantly, the cells populating the collagen scaffolds maintained expression of biliary markers such as CK19, CK7, HNF1b, Sox9 and CFTR (Supplementary Fig 15f-15g) and exhibited GGT and ALP enzymatic activity (Supplementary Fig 15h-15i). Primary epithelial cells of different origin (human mammary epithelial cells; HMEC) failed to survive and adequately populate densified collagen tubes under the same conditions (Supplementary Fig. 16a). Moreover, plated HMECs failed to survive in a 10% (vol/vol) bile solution compared to ECOs (Supplementary Fig. 16b), further confirming that ECOs constitute the only cell type capable of generating bile resistant bio-engineered bile ducts. Collectively, these results demonstrate the capacity of ECOs for populating tubular densified collagen scaffolds without losing their original characteristics.

**Supplementary discussion**

Our system provides proof-of-principle for the application of primary cells in regenerative medicine; however, the use of stem cells has been suggested as an alternative for cell based therapy. Although we have recently established a system

for the generation of stem cell-derived cholangiocyte-like cells (CLCs) (3), there are significant differences between ECOs and CLCs that render ECOs better suited to regenerative therapies for extrahepatic biliary injury. CLCs correspond to intrahepatic cholangiocytes, while ECOs represent extrahepatic biliary epithelium. These two cell types are distinct in terms of embryological origin and disease involvement (4). Furthermore, CLCs still express fetal markers and therefore are more immature compared to ECOs derived from primary cells (3). Therefore, CLCs may require a period of adjustment and further maturation in vivo, while mature, functional cells, such as ECOs, are required for coping with biliary injury in the acute setting. Finally, although hIPSCs provide a very good source of cells capable of generating almost any tissue, fully differentiated CLCs cannot be expanded; initial derivation/ characterization of hIPSC lines remains time consuming; while variability in capacity of differentiation still constitutes a challenge. ECOs can be derived in less than 24 hours with a very high efficiency and can be expanded for multiple passages without losing their original characteristics. Consequently, ECOs are comparable to CLCs in terms of scalability, while their mature phenotype provides a unique advantage for regenerative medicine applications in the context of tissue repair.

**Supplementary References**

1.  Chan, B. P. & Leong, K. W. Scaffolding in tissue engineering: general approaches and tissue-specific considerations. *Eur. Spine J.* **17,** 467–479 (2008).

2.  Cheung, H.-Y., Lau, K.-T., Lu, T.-P. & Hui, D. A critical review on polymer-based bio-engineered materials for scaffold development. *Compos. Part B*

*Eng.* **38,** 291–300 (2007).

3. Sampaziotis, F. *et al.* Cholangiocytes derived from human induced pluripotent stem cells for disease modeling and drug validation. *Nat. Biotechnol.* 1–11 (2015). doi:10.1038/nbt.3275

4. Tabibian, J. H., Masyuk, A. I., Masyuk, T. V., O'Hara, S. P. & LaRusso, N. F. Physiology of cholangiocytes. *Compr. Physiol.* **3,** 541–565 (2013).

**Supplementary Figure 1**

Screening for optimal conditions for the isolation and propagation of extra-hepatic cholangiocytes **(a)** Mean viability ratio following isolation of primary cholangiocytes with different methods. C+D: Collagenase + Dispase. Error bars, SD; n=3. Asterisks represent statistically significant differences in viability ratio between mechanical dissociation and other isolation methods; ***$P<0.001$, ****$P<0.0001$; one-way ANOVA with Dunnett correction for multiple comparisons **(b)** Mean number of resulting cells following 7 days of culture with various growth factors. E: Epidermal Growth Factor, R: R-spondin, D: DKK-1, IL6: Interleukin-6, HGF: Hepatocyte Growth Factor, VEGF: Vascular Endothelial Growth Factor, FBS: Foetal Bovine serum, F2: Fibroblast Growth Factor (FGF) 2, F7: FGF-7, F10: FGF-10, A: Activin-A, SB: Activin inhibitor SB-431542. Error bars, SD; n=3. Asterisks represent statistically significant differences in the number of resulting cells between E+R+D and other culture conditions; ****$P<0.0001$; one-way ANOVA with Dunnett correction for multiple comparisons **(c)** Representative live images of freshly isolated primary cholangiocytes grown under different culture conditions for 7 days. EGF: Epidermal Growth Factor. Scale bars: 500 µm. **(d)** Western blot analyses demonstrating increased levels of phosphorylated β-catenin in ECOs treated with R-spondin and DKK vs. R-spondin alone or R-spondin and the GSK-3 inhibitor CHIR 99021 (CHIR), used as a positive control. **(e)** Quantification of the western blot demonstrated in panel **(d)**. **(f)** ECOs treated with R-spondin and DKK exhibit increased Rho Kinase activity, consistent with non-canonical Wnt signalling/ PCP pathway activation. Error bars: SD; ****$P<0.0001$; one way anova with Dunnett correction for multiple comparisons; n=3; Y-27632: Rho Kinase inhibitor Y-27632.

1 **Supplementary Figure 2**

2 ECOs represent a highly homogeneous population of epithelial CK19+/CK7+ cells,

3 with minimal mesenchymal contamination. Flow cytometry analyses demonstrating

4 the expression of the biliary markers CK7 and CK19 but not the mesenchymal

5 marker vimentin (VIM) in freshly isolated primary cholangiocytes (Primary) and

6 Passage 20 (P20) ECOs, n=3. Fibroblasts are used as a positive control for

7 mesenchymal markers.

8

9 **Supplementary Figure 3**

10 Characterization of ECO lines derived from the gallbladder and common bile duct

11 brushings. **(a)** Schematic representation of the method for the derivation of ECOs

12 from the gallbladder. **(b)** Schematic representation of the method for the derivation of

13 ECOs from common bile duct brushings. **(c)** Quantitive real time PCR (QPCR)

14 confirming the expression of biliary markers in Passage 20 (P20) organoids of 2

15 ECO lines derived from common bile duct brushings (ECO_BR) and the gallbladder

16 (ECO_GB). Freshly isolated cholangiocytes (Primary) are used as a positive control,

17 n=4 biological replicates. Center line, median; box, interquartile range (IQR);

18 whiskers, range (minimum to maximum). Values are relative to the housekeeping

19 gene Hydroxymethylbilane Synthase (*HMBS*). **(d)** Immunofluorescence (IF) analyses

20 confirming the expression of biliary markers in P20 ECO_BR and ECO_GB

21 organoids. Scale bars: 100 μm. **(e)** ALP staining of P20 ECO_BR and ECO_GB

22 organoids. Scale bars: 500μm. **(f)** Mean GGT activity of P20 ECO_BR and ECO_GB

23 vs. primary cholangiocytes; n=3; error bars, SD. These data are complementary to

24 the data shown in Figures 1 and 2.

6

**Supplementary Figure 4**

Genetic stability of ECOs following long-term in vitro culture for 20 passages. **(a)** Growth curves of 3 different ECO lines cultured in vitro for 20 passages. **(b)** Normal Karyotype of ECOs at P20; n=3. **(c)** Comparative Genomic Hybridization analyses comparing ECOs at Passage 1 (red) and P20 (blue), demonstrating genomic stability *in vitro*; n=3.


**Supplementary Figure 5**

ECOs exhibit ultra-structural features characteristic of cholangiocytes. Transmission electron microscopy image demonstrating the presence of microvilli (white arrowheads) and tight junctions (black arrowheads) in passage 20 ECO cells. Scale bar: 2µm.


**Supplementary Figure 6**

ECOs express markers biliary markers. **(a-b)** Single channel **(a)** and high magnification **(b)** images of the IF analyses demonstrated in Figure 1f demonstrating the expression of biliary markers by ECOs. Scale bars: 100µm. These data are complementary to the data shown in Figure 1.


**Supplementary Figure 7**

ECOs do not express markers of other lineages. **(a)** IF images demonstrating the lack of expression of stem cell markers or markers of other lineages (liver, pancreas) by ECOs. Scale bars: 100μm **(b)** IF images demonstrating appropriate positive controls expressing the markers demonstrated in **(a)**. **(c)** QPCR analyses demonstrating the lack of expression of stem cell markers or markers of other lineages (liver, pancreas) by ECOs. Stel, activated stellate cells; Fibro, fibroblasts; HEP, primary human freshly plated hepatocytes; Panc, primary human pancreatic cells; ES, embryonic stem cells; HB, hIPSC-derived hepatoblasts; SC, ECO populated scaffolds; Int. Org., Intestinal Organoids; n=4 biological replicates; n=3 biological replicates for POU5F1, NANOG, PROM1. Center line, median; box, interquartile range (IQR); whiskers, range (minimum to maximum). Values are relative to the housekeeping gene Hydroxymethylbilane Synthase (*HMBS*).

**Supplementary Figure 8**

Transcriptomic profile analyses of ECOs. **(a)** Euclidean hierarchical clustering analysis comparing the transcriptome of ECOs across multiple passages (P1, P10, P20) and Embryonic Stem (ES) cells used as a negative control, focusing on genes that define the transcriptional signature of ECOs (4513 genes differentially expressed between ECOs and ES cells). For each probe, standard scores (z-scores) indicate the differential expression measured in number of standard deviations from the average level across all the samples, n=3. **(b)** Heatmap showing the Pearson correlation coefficient (r) of the global gene expression between ECOs across multiple passages (P1, P10, P20), freshly isolated primary cholangiocytes (PCs), hIPSC-derived intrahepatic Cholangiocyte Like Cells (iChoLC), primary hepatocytes

(HEPs) and ES used as a negative control, n=3. The analysis was performed focusing on all probes detected in all 3 biological replicates. **(c)** Heatmap showing the expression of representative biliary, hepatic and stem cell markers between passage 20 ECOs (ECOs), PCs, HEPs and ES cells; n=3; z-scores as in **(a)**. **(c)** Principal Component Analysis (PCA) between ECOs, PCs, iChoLC, HEPs and ES cells, n=3. The analysis was performed using all probes detected in all 3 replicates. ECOs cluster closely with primary cholangiocytes for component 1 accounting for 41% of total variability. **(d)** Gene ontology (GO) analyses focusing on the genes differentially expressed between PCs and ECOs in Figure 1g; n=3. Characteristic GO terms from each cluster are provided ($P<0.05$). Terms associated with the biliary epithelium are identified only in the common cluster.

**Supplementary Figure 9**

ECOs injected under the kidney capsule of immune compromised mice form tubular structures expressing biliary markers, but do not demonstrate spontaneous differentiation in other lineages. **(a)** Schematic representation of the method used for the injection of ECOs. **(b)** Image of an excised kidney transplanted with ECOs; scale bar: 500µm. **(c)** Cross-section of a transplanted kidney demonstrating the formation of tubular structures; scale bar: 500µm. **(d)** IF images demonstrating the formation of tubular structures by the engrafted cells expressing the biliary marker CK7 and a human-specific Ku80 epitope, but not expressing stem cell markers or markers of other lineages (liver, pancreas). Scale bars: 100µm.

**Supplementary Figure 10**

Generation of ECOs expressing Green Fluorescent Protein (GFP). **(a)** Flow cytometry analyses demonstrating the generation of a homogeneous population of GFP-ECOs following lentiviral transduction and flow sorting. **(b)** Confocal microscopy images demonstrating the generation of fully grown GFP-ECO organoids from a single GFP-expressing cell. Scale bars: 100 µm. Images are representative.

**Supplementary Figure 11**

ECOs dissociated to single cells (ECO-SCs) can populate biodegradable PGA scaffolds. **(a,b)** Photographs of a PGA scaffold before **(a)** and after **(b)** treatment with ECOs. Scale bars: 1cm. **(c)** Light microscopy images of a PGA scaffold populated with ECO-SCs. Red arrowheads: Fully populated scaffold; black arrowheads: cells recruiting new PGA fibers; white arrowheads: PGA fibers. Scale bars: 100µm. **(d)** Confocal microscopy images demonstrating cell expansion at different time-points after seeding of GFP-positive ECO-SCs on a PGA scaffold. White lines indicate the position of PGA fibers. Scale bars: 100µm. **(e)** IF demonstrating the expression of biliary markers and lack of EMT markers in ECO-SCs seeded on PGA scaffolds. Scale bars: 50µm **(f)** QPCR analyses demonstrating the expression of biliary markers in ECOs before (ECOs) and after (scaffold) seeding on PGA scaffolds, n=4 biological replicates. Center line, median; box, interquartile range (IQR); whiskers, range (minimum to maximum). Values are relative to the housekeeping gene Hydroxymethylbilane Synthase (*HMBS*). **(g)** Ratio of CK7+/CK19+ and CK19+/Vimentin (VIM)+ cells in randomly selected IF images similar to the image shown in **(e)**; n=6. **(h)** Mean GGT activity of ECO-SCs populating a PGA scaffold,

n=4. Error bars represent SD. ****$P$<0.001 (two-tailed t-test). **(i)** ALP staining of PGA scaffolds populated by ECO-SCs. Scale bars: 500µm.

**Supplementary Figure 12**

2D plated cholangiocytes fail to populate PGA scaffolds. **(a)** Growth curves of primary cholangiocytes plated as monolayer (2D) vs. primary cholangiocytes grown as ECOs (ECO), demonstrating that 2D cholangiocytes stop proliferating after a few passages. Starting from the same number of cells ($5 \times 10^5$) 2D cholangiocytes fail to provide the number of cells required to seed a PGA scaffold ($10^7$ cells). **(b)** Brightfield images demonstrating that 2D cholangiocytes fail to expand and populate PGA scaffolds and remain limited to the site of injection. A brightfield image of a scaffold populated by ECOs dissociated to single cells (ECO-SC) is provided as a positive control. The scaffold was seeded with same number of cells and cultured for the same period of time as the 2D cholangiocyte scaffold. Scale bars: 100µm.

**Supplementary Figure 13**

Fibroblast-populated scaffolds fail to reconstruct the gallbladder following transplantation in EHBI mice. **(a)** Flow cytometry analyses demonstrating the generation of a homogeneous population of GFP-expressing Fibroblasts (GFP-Fibro) following lentiviral transduction. **(b)** IF images demonstrating the expression of GFP in fibroblasts following lentiviral transduction. Scale bars: 100µm. **(c, d)** Brightfied **(c)** and confocal microscopy **(d)** images demonstrating the generation of fibroblast populated PGA scaffolds. Scale bars: 100µm. **(e,f)** Postmortem images of

transplanted EHBI mice demonstrating failure to reconstruct the gallbladder with fibroblast-populated scaffolds. The site of reconstruction can only be identified by the presence of non-absorbable sutures (white arrowheads). Scale bars: 1mm. **(g)** Image of a gallbladder transplanted with a fibroblast-populated scaffold demonstrating failure to reconstruct the organ, abnormal morphology more consistent with a fibrotic mass and lack of a bile filled lumen. Scale bars: 1mm. **(h)** T2 phase Magnetic Resonance Images (MRI; axial plane) demonstrating the absence of a bile filled lumen in a gallbladder transplanted with a fibroblast populated scaffold. The white signal consistent with bile is identified up to the cystic duct but not at the site of the transplanted gallbladder. **(i)** H&E images demonstrating replacement of the gallbladder epithelium by fibroblasts and obliteration of the gallbladder lumen. **(j)** IF analyses demonstrating the abscence of GFP-expressing cells in the transplanted gallbladders, the lack of epithelial markers and the presence of connective tissue markers, Scale bars: 100μm.

**Supplementary Figure 14**

Characterization of ECO-reconstructed gallbladders in extrahepatic biliary injury (EHBI) mice. **(a)** Postmortem images of mice receiving acellular PGA scaffolds (scaffold only), healthy control mice (not transplanted) and mice receiving ECO-populated PGA scaffolds (transplanted). The yellow pigmentation of the peritoneal cavity (top, white dashed line) and seminal vesicles (bottom, black dashed line) is consistent with bile leak in the 'scaffold only' group. Scale bars: 5mm **(b)** Post mortem images demonstrating the reconstructed gallbladders in situ (n=3). Black arrows: sutures; L: liver; scale bars: 1mm. **(c)** IF images of the transplanted

scaffolds, corresponding to figure 3e, demonstrating GFP-positive cells expressing human (Ku80) and biliary markers (CK19, CK7, CFTR) integrated in the reconstructed biliary epithelium; the presence of mouse stromal cells expressing vimentin and mouse endothelial cells expressing CD31; and the presence of GFP+, CK19-, Vimentin+ cells integrated in connective tissue of the reconstructed organ. Scale bars: 100µm. **(d)** QPCR analyses using human-specific primers confirming expression of biliary markers by transplanted ECO-populated scaffolds (ECOs in vivo) compared ECOs in vitro and mouse gallbladder used as a negative control, n=4 replicates. Center line, median; box, interquartile range (IQR); whiskers, range (minimum to maximum). Values relative to *HMBS* expression. **(e)** Ratio of CK19+/CK7+, CK19+/GFP+ and Vimentin (VIM)/GFP+ cells  quantified in randomly selected sections of transplanted ECO-populated scaffolds; n=18. **(f)** T1&T2 vs. T2 phase Magnetic Resonance Images (MRI; axial plane) demonstrating bile in the lumen of a reconstructed gallbladder (white signal) and a patent cystic duct relative to the surrounding liver (n=2). GB: Gallbladder; CD: Cystic Duct; L: Liver parenchyma.

**Supplementary Figure 15**

ECOs can populate densified collagen tubular scaffolds. **(a)** Schematic representation of the method used. **(b)** Image of a densified collagen construct prior to tube excision. Scale bar, 500µm. **(c)** Maximum intensity projection image demonstrating a GFP+ ECO-populated tube after its generation. Scale bar; 10µm **(d)** Confocal microscopy image demonstrating lumen patency of an ECO-populated collagen tube. Scale bar; 10µm. **(e)** Images of a near confluent GFP+ ECO-tube. Scale bar; 100µm. **(f)** IF analyses demonstrating the expression of biliary markers by

ECOs following the generation of ECO-tubes. Scale bar; 100µm. **(g)** QPCR analyses

demonstrating the expression of biliary markers before (ECOs) and after (Scaffold)

the generation of ECO-populated collagen tubes. ES cells are used as a negative

control, n=4 replicates. Center line, median; box, interquartile range (IQR); whiskers,

range (minimum to maximum). Values are relative to *HMBS* expression. **(h, i)** ECO-

tubes exhibit ALP **(h)** and GGT **(i)** activity. Scale bars, 500µm; MEFs, Mouse

Embryonic feeders used as negative control; Scaffold, ECO-populated, densified

collagen tubes; error bars, SD; n=3.


**Supplementary Figure 16**

Primary human mammary epithelial cells (HMECs) lack the capacity to adequately

populate densified collagen scaffolds or survive in the environment of primary

cholangiocytes. **(a)** Light microscopy images demonstrating failure of HMECs survive

and adequately populate collagen tubular scaffolds. Scale bar: 100µm. **(b)** Flow

cytometry analysis demonstrating survival of ECOs vs. plated HMECs following

exposure to a 10% (vol/vol) bile solution.


**Supplementary Figure 17**

Survival analysis and characterization of ECO-populated densified collagen tubes.

**(a)** H&E staining demonstrating the presence of a biliary epithelium and a patent

lumen in ECO-tubes. The images are complementary to Figure 4e **(b)** IF analyses

demonstrating the expression of human specific (Ku80), biliary (CK19, CK7, CFTR),

stromal (Vimentin, VIM) and vascular (CD31) markers in transplanted bio-tubes

populated with GFP+ ECOs. Apoptosis (TUNEL) and proliferation (Ki67) markers are

**Supplementary Video 1**

Magnetic Resonance Cholangio-Pancreatography (MRCP, sagital plane) of an Extrahepatic Biliary Injury (EHBI) mouse 104 days following biliary reconstruction with an ECO-populated scaffold. The T2 weighed image sequence demonstrates the presence of bile in the lumen of a reconstructed gallbladder (high intensity white signal) and a patent cystic duct. The surrounding tissues are characterized by low intensity signal and appear dark. To assess the anatomy of the surrounding organs

please refer to supplementary video 2 for a T1 weighed Magnetic Resonance Imaging sequence.

**Supplementary Video 2**

T1 weighed Magnetic Resonance Imaging (MRI) (coronal plane) of an Extrahepatic Biliary Injury (EHBI) mouse 104 days following biliary reconstruction with an ECO-populated scaffold. This image sequence is optimal for demonstrating the anatomy of the tissue surrounding the reconstructed gallbladder and biliary tree. However, water, water-rich tissues and bile are characterized by low intensity signal, appear dark and may be difficult to identify

**Supplementary video 3**

Time lapse images demonstrating the generation of a fully grown organoid from a single cell.

**Supplementary table 1**

2 Donor demographics, corresponding to 8 different ECO lines. DCD: Donation after

3 Circulatory Death, DBD: Donation after Brain Death, F: Female, M: male, CBD:

4 Common Bile Duct, GB: Gallbladder, BR: CBD Brushings

5

| Donor type | Blood Group | Age (years) | Gender | Site |
|------------|-------------|-------------|--------|------|
| DCD | O- | 33 | F | CBD |
| DBD | O+ | 56 | F | CBD |
| DCD | A- | 77 | M | CBD |
| DBD | O+ | 57 | M | CBD, GB |
| DCD | O- | 44 | M | CBD, GB |
| DCD | O+ | 48 | M | CBD |
| DBD | A+ | 36 | M | BR |
| DBD | B+ | 48 | F | BR |

6

7

8

9 **Supplementary table 2**

10 Microarray gene expression data corresponding to the heat map in Figure 1g

1  **Supplementary Table 3:** List of antibodies used

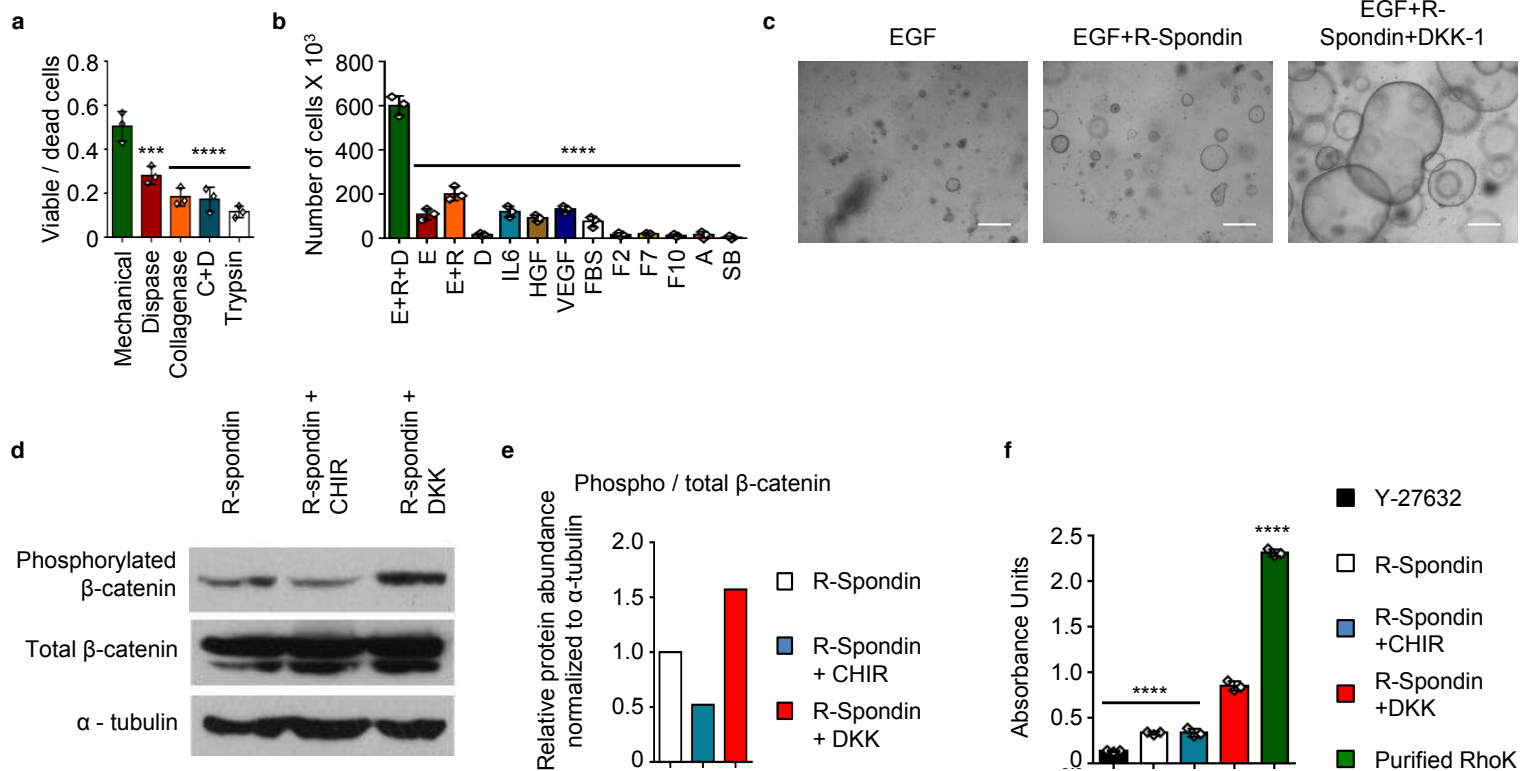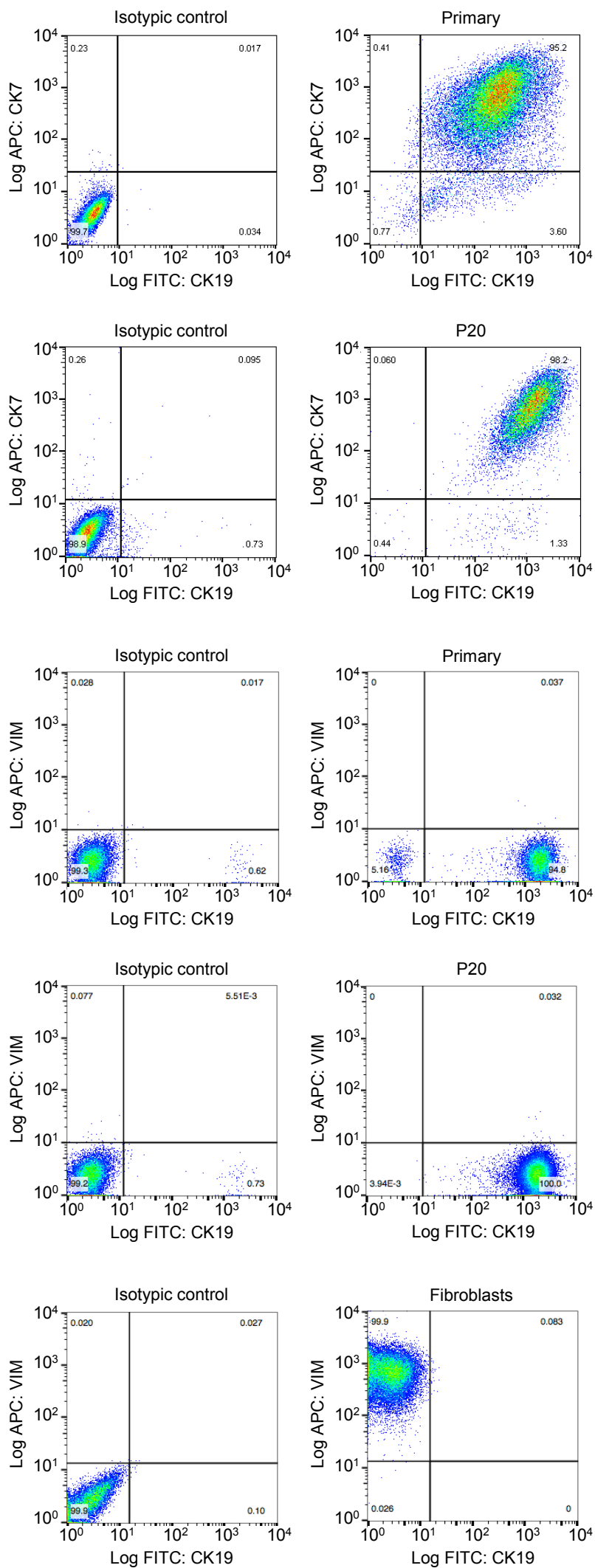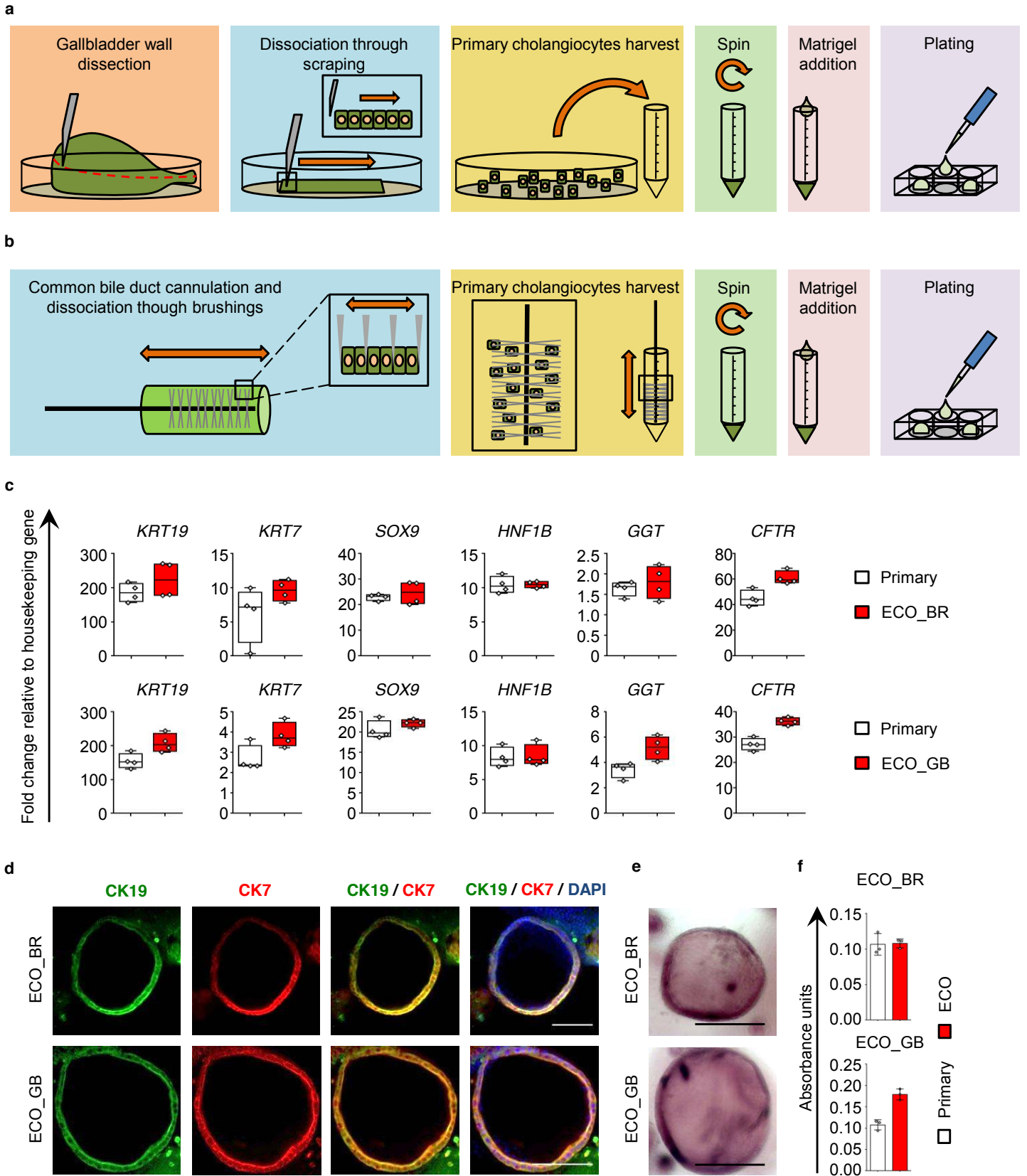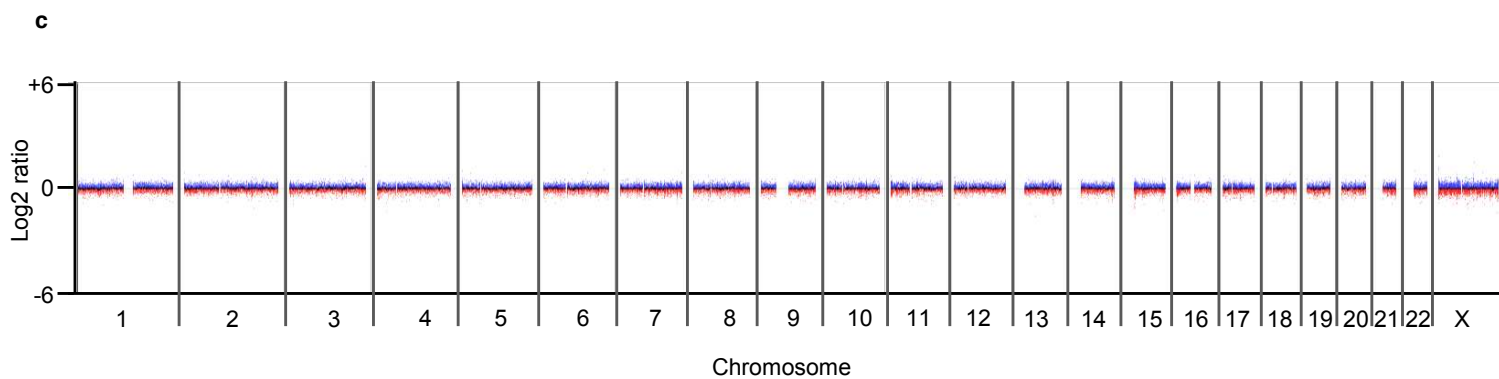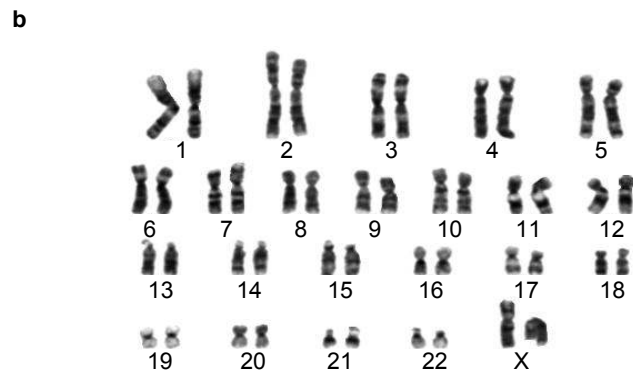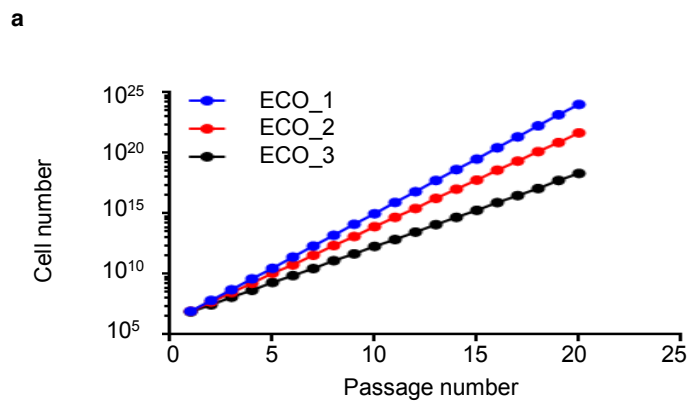| Target protein | Dilution | Company | Cat Number |
|---|---|---|---|
| CYTOKERATIN 19 | 1:100 | ABCAM | ab7754 |
| CYTOKERATIN 19 (KRT19) | 1:50 | DSHB | TROMA-III |
| SOX9 H-90 | 1:100 | SANTA CRUZ | sc-20095 |
| HNF1B (c-20) | 1:100 | SANTA CRUZ | sc-7411 |
| CYTOKERATIN 7 (RCK105) | 1:100 | ABCAM | ab9021 |
| CYTOKERATIN 7 | 1:100 | ABCAM | ab68459 |
| CYSTIC FIBROSIS TRANSMEMBRANE CONDUCTANCE REGULATOR (CFTR) | 1:100 | SANTA CRUZ | sc-10747 |
| GAMMA GLUTAMYL TRANSPEPTIDASE (GGT) | 1:100 | ABCAM | ab55138 |
| SOMATOSTATIN RECEPTOR 2 | 1:100 | ABCAM | ab134152 |
| SECRETIN RECEPTOR (C-20) | 1:100 | SANTA CRUZ | sc-26633 |
| SECRETIN RECEPTOR | 1:100 | ABCAM | ab85565 |
| ASBT (C14) | 1:100 | SANTA CRUZ | sc-27493 |
| STEM101 HUMAN KU80 CELL NUCLEUS MARKER | 1:100 | STEM CELLS INC. | Y40400 |
| ALEXA FLUOR DONKEY ANTI-Rabbit 568 | 1:1000 | INVITROGEN | A10042 |
| ALEXA FLUOR DONKEY ANTI-Rabbit 488 | 1:1000 | INVITROGEN | A21206 |
| ALEXA FLUOR DONKEY ANTI-Rabbit 647 | 1:1000 | INVITROGEN | A31573 |
| ALEXA FLUOR DONKEY ANTI-goat 568 | 1:1000 | INVITROGEN | A11057 |
| ALEXA FLUOR DONKEY ANTI-goat 488 | 1:1000 | INVITROGEN | A11055 |
| ALEXA FLUOR DONKEY ANTI-goat 647 | 1:1000 | INVITROGEN | A21447 |
| ALEXA FLUOR DONKEY ANTI-mouse 568 | 1:1000 | INVITROGEN | A10037 |
| ALEXA FLUOR DONKEY ANTI-mouse 488 | 1:1000 | INVITROGEN | A21202 |
| ALEXA FLUOR DONKEY ANTI-mouse 647 | 1:1000 | INVITROGEN | A31571 |

2

3

4

1 **Supplementary table 4:** List of primers used

| Gene | | Primer sequence (5' à 3') | Gene | | Primer sequence (5' à 3') |
|---|---|---|---|---|---|
| HNF1B | F | TCACAGATACCAGCAGCATCAGT | CK7 | F | GATTGCTGGCCTTCGGGGT |
| | R | GGGCATCACCAGGCTTGTA | | R | TCATCACAGAGATATTCACGGCTC |
| PBGD | F | GGAGCCATGTCTGGTAACGG | GGT | F | GTGAGAGCAGTTGGCTGTGC |
| | R | CCACGCGAATCACTCTCATCT | | R | GTTGAACTCTGCTGTGGGGC |
| SOX9 | | Hs_SOX9_1_SG QuantiTect Primer Assay (Quiagen, Cat Number: QT00001498) | CFTR | F | AGTTGCAGATGAGGTTGGGC |
| | | | | R | AAAGAGCTTCACCCTGTCGG |
| CK19 | F | ACGACCATCCAGGACCTGCGG | SCR | F | TGCTCACCAGCAGAAATGGT |
| | R | TCCCACTTGGCCCCTCAGCGTA | | R | AGGTAGGAGTGCCGCTTCTC |
| AQPR1 | F | GGCCAGCGAGTTCAAGAAGAA | SSTR | F | GAAAAGCAAAGATGTCACACTGGA |
| | R | TCACACCATCAGCCAGGTCAT | | R | TTGGCATAGCGGAGGATGAC |

2

**a**

Viable / dead cells

Mechanical, Dispase, Collagenase, C+D, Trypsin

*** ****

**b**

Number of cells X 10³

E+R+D, E, E+R, D, IL6, HGF, VEGF, FBS, F2, F7, F10, A, SB

****

**c**

EGF    EGF+R-Spondin    EGF+R-Spondin+DKK-1

**d**

Phosphorylated β-catenin

Total β-catenin

α - tubulin

R-spondin    R-spondin + CHIR    R-spondin + DKK

**e**

Phospho / total β-catenin

Relative protein abundance normalized to α-tubulin

☐ R-Spondin
■ R-Spondin + CHIR
■ R-Spondin + DKK

**f**

Absorbance Units

****    ****

■ Y-27632
☐ R-Spondin
■ R-Spondin +CHIR
■ R-Spondin +DKK
■ Purified RhoK

**Sampaziotis et al. Supplementary Figure 2**

**a**



**b**



**c**

**Sampaziotis et al. Supplementary Figure 6**

**a**



**b**

Fibroblasts     Hepatocytes     Pancreatic progenitors     hIPSCs     Sigmoid colon organoid

**Sampaziotis et al. Supplementary Figure 8**

a



b



c



d

**a**



Non GFP ECOs

GFP ECOs

**b**



Single cells

0 days

Fully grown

7-14 days

a

b

c

d

48hrs          2 weeks          4 weeks

e

CK19          CK7          VIMENTIN          CK19 / CK7 / VIMENTIN / DAPI

f

Fold change relative to housekeeping gene

*KRT7*          *KRT19*          *HNF1B*

*SOX9*          *GGT*          *CFTR*

□ ECOs          ■ Scaffold

g

Ratio

□ CK19/VIM
■ CK7/CK19

h

Absorbance units

□ Substrate          ■ Scaffold

i

Unstained

ALP staining

**a**



**b**

2D cholangiocyte populated scaffold

ECO-populated scaffold

**Sampaziotis et al. Supplementary Figure 13**

a



b



c



d



e



f



g



h



i



j

| GFP | S100A4 | CK19 | GFP / S100A4 / CK19 / DAPI |

**a**

Scaffold only · Not transplanted · Transplanted

Seminal vesicles

**b**

Mouse 1 · Mouse 2 · Mouse 3

**c**

GFP / CK19 / CK7 / DAPI · GFP / Ku80 / DAPI · GFP / Ku80 / DAPI · GFP / CFTR / DAPI · GFP / CK19 / Vimentin / DAPI · GFP / Vimentin / CD31 / DAPI

**d**

CK19 · CK7 · HNF1B · Sox9 · CFTR

Fold change relative to housekeeping gene

□ ECOs in vitro   ■ ECOs in vivo   ■ Mouse

**e**

CK19/CK7 · CK19/GFP · VIM/GFP

**f**

T2 · T1 & T2

**a**

Scaffold mould    Addition of collagen    Densification complete    Removal of scaffold    Tube excision

Absorbent    Absorption of water from collagen gel

Collagen tube scaffold

**b**



**c**    **d**    **e**



**f**

CK19 / CK7 / DAPI



**g**

Fold change relative to housekeeping gene

CK19    CK7    HNF1B

CFTR    SOX9

☐ ES cells
🟥 ECOs
🟩 Scaffold

**h**

Unstained    ALP



**i**

Absorbance units

☐ Substrate only
⬛ MEFs
🟥 ECOs
🟩 Primary Cholangiocytes
🟦 Scaffold

**a**



**b**

**Sampaziotis et al. Supplementary Figure 17**



a

b

GFP / CK19 / DAPI  |  GFP / CK19 / CK7 / DAPI  |  GFP / CFTR / DAPI  |  GFP / VIM / CD31 / DAPI  |  GFP / TUNEL / Ki67 / DAPI  |  GFP / Ku80 / CK7 / DAPI

c

TUNEL  |  S100A4  |  Ki67  |  TUNEL / DAPI  |  Ki67 / DAPI  |  GFP / VIM / CD31 / DAPI

d

**Survival curve**

% surviving

Fibroblasts
ECOs
Untreated

Days

****

Number of mice at risk

| Days | 0 | 1 | 3 | 4 | 5 | 19 | 27 | 31 |
|---|---|---|---|---|---|---|---|---|
| Untreated | 4 | 4 | 0 | 0 | 0 | 0 | 0 | 0 |
| Fibro | 4 | 4 | 0 | 0 | 0 | 0 | 0 | 0 |
| ECOs | 11 | 11 | 11 | 9 | 8 | 7 | 6 | 5 |

e

ALP  |  Bili  |  ALT

CTRL / ECOs / BDL

f

SC  L